J Neurophysiol 120: 394–408, 2018.
First published April 11, 2018; doi:10.1152/jn.00691.2017.

RESEARCH ARTICLE | *Cellular and Molecular Properties of Neurons*

Functional roles of Kv1-mediated currents in genetically identified subtypes of pyramidal neurons in layer 5 of mouse somatosensory cortex

Dongxu Guan, Dhruba Pathak, and Robert C. Foehring
Department of Anatomy and Neurobiology, University of Tennessee Health Science Center, Memphis, Tennessee

Submitted 20 September 2017; accepted in final form 3 April 2018

Guan D, Pathak D, Foehring RC. Functional roles of Kv1-mediated currents in genetically identified subtypes of pyramidal neurons in layer 5 of mouse somatosensory cortex. *J Neurophysiol* 120: 394–408, 2018. First published April 11, 2018; doi:10.1152/jn.00691.2017.—We used voltage-clamp recordings from somatic outside-out macropatches to determine the amplitude and biophysical properties of putative Kv1-mediated currents in layer 5 pyramidal neurons (PNs) from mice expressing EGFP under the control of promoters for *etv1* or *glt*. We then used whole cell current-clamp recordings and Kv1-specific peptide blockers to test the hypothesis that Kv1 channels differentially regulate action potential (AP) voltage threshold, repolarization rate, and width as well as rheobase and repetitive firing in these two PN types. We found that Kv1-mediated currents make up a similar percentage of whole cell K^+ current in both cell types, and only minor biophysical differences were observed between PN types or between currents sensitive to different Kv1 blockers. Putative Kv1 currents contributed to AP voltage threshold in both PN types, but AP width and rate of repolarization were only affected in *etv1* PNs. Kv1 currents regulate rheobase, delay to the first AP, and firing rate similarly in both cell types, but the frequency-current slope was much more sensitive to Kv1 block in *etv1* PNs. In both cell types, Kv1 block shifted the current required to elicit an onset doublet of action potentials to lower currents. Spike frequency adaptation was also affected differently by Kv1 block in the two PN types. Thus, despite similar expression levels and minimal differences in biophysical properties, Kv1 channels differentially regulate APs and repetitive firing in *etv1* and *glt* PNs. This may reflect differences in subcellular localization of channel subtypes or differences in the other K^+ channels expressed.

NEW & NOTEWORTHY In two types of genetically identified layer 5 pyramidal neurons, α-dendrotoxin blocked approximately all of the putative Kv1 current (on average). We used outside-out macropatches and whole cell recordings at 33°C to show that despite similar expression levels and minimal differences in biophysical properties, Kv1 channels differentially regulate action potentials and repetitive firing in *etv1* and *glt* pyramidal neurons. This may reflect differences in subcellular localization of channel subtypes or differences in the other K^+ channels expressed.

potassium channel; repetitive firing; somatosensory cortex

INTRODUCTION

Pyramidal neurons (PNs) are the most numerous components in neocortical circuitry, and there is increasing evidence that PN properties vary with cortical layer and synaptic targets. PNs in layer 5 have been classified on the basis of morphology and laminar position, projection patterns, and firing patterns (Chagnac-Amitai et al. 1990; Christophe et al. 2005; Dembrow et al. 2010; Hattox and Nelson 2007; Ivy and Killackey 1982; Kasper et al. 1994; Larkman and Mason 1990; Le Bé et al. 2007; Mason and Larkman 1990; Tseng and Prince 1993; Wise and Jones 1977). In somatosensory cortex, there is high concordance of these different schemes: large, thick-tufted PNs in deep layer 5 project beyond the telencephalon (pyramidal tract or PT type), and thin-tufted PNs in superficial layer 5 project within the telencephalon (intratelencephalic or IT type; Reiner et al. 2003, 2010; Shepherd 2013). PT-type PNs typically have narrower action potentials (APs), have a greater tendency to fire in short, high-frequency onset bursts, and fire rapidly with little spike frequency adaptation (SFA; Brown and Hestrin 2009; Dembrow et al. 2010; Hattox and Nelson 2007; Le Bé et al. 2007; Sheets et al. 2011; Suter et al. 2013). We studied layer 5 PNs identified by enhanced green fluorescent protein (EGFP) expression (Bishop et al. 2015; Guan et al. 2015; Pathak et al. 2016) in BAC mice under control of either the *etv1* or *glt* genes (Gong et al. 2002, 2003, 2007). *Etv1* PNs are IT-type PNs and are located more superficially in layer 5 than *glt* PNs, which are a subgroup of PT-type neurons (Bishop et al. 2015; Groh et al. 2010; Guan et al. 2015; Kim et al. 2015; Pathak et al. 2016). *Etv1* and *glt* PNs also differ in morphology and projection targets (Groh et al. 2010).

Consistent with *etv1* PNs being a subset of IT-type and *glt* being a subset of PT-type PNs (Christophe et al. 2005; Dembrow et al. 2010; Groh et al. 2010; Hattox and Nelson 2007; Le Bé et al. 2007; Sheets et al. 2011; Suter et al. 2013), *etv1* PNs have broader APs, fire more slowly and with lower gain to direct current (DC) inputs, and exhibit more SFA than *glt* PNs (Groh et al. 2010; Guan et al. 2015). *Etv1* PNs also have higher rheobase compared with *glt* (Guan et al. 2015). Different PN types within layer 5 are likely to have distinct functions, although our present understanding is limited. For example, prolonged exposure to anesthesia before brain removal elicits burst firing in PT-type layer 5 PNs but not in IT-type cells (Christophe et al. 2005), and IT-type PNs mediate cortical responses to antidepressants, whereas *glt* PNs do not (Schmidt et al. 2012).

Previously, we showed differences in firing rate, gain to DC input, and SFA between *etv1* and *glt* PNs due to greater expression of the slow afterhyperpolarization (sAHP) current

Address for reprint requests and other correspondence: R. C. Foehring, Dept. of Anatomy and Neurobiology, University of Tennessee Health Science Center, 855 Monroe Ave., Memphis, TN 38163 (e-mail: rfoehrin@uthsc.edu).

in *etv1* PNs. The sAHP current is almost absent from *glt* PNs, which in contrast have greater expression of small-conductance Ca^{2+}-activated K^+ channel (SK)-mediated medium AHP current (Guan et al. 2015). Rodent PNs also express several voltage-gated K^+ channels (Kv) that could differentially regulate firing in different types of PNs. These Kv currents have both transient and persistent components in PNs (Bekkers 2000a, 2000b; Foehring and Surmeier 1993; Korngreen and Sakmann 2000; Locke and Nerbonne 1997). The persistent currents in PNs are mostly due to expression of Kv1, Kv2 (the largest component), and Kv7 channels (Bekkers and Delaney 2001; Bishop et al. 2015; Guan et al. 2006, 2007a, 2007b, 2011a, 2011b, 2013, 2015; Murakoshi and Trimmer 1999). A key difference between *etv1* and *glt* PNs is the relative expression of Kv2-mediated current, which is larger in *glt* than in *etv1* PNs (~62% vs. 30% of whole cell current; Bishop et al. 2015). Also, *etv1* PNs express Kv2.1 and Kv2.2 currents in approximately equal proportions, whereas *glt* PNS only express Kv2.1 currents (Bishop et al. 2015). *Glt* PNs fire faster than *etv1* PNs, consistent with a permissive role for Kv2 channels to support high-rate repetitive firing (Du et al. 2000; Guan et al. 2013; Hönigsperger et al. 2017; Johnston et al. 2008; Liu and Bean 2014).

Our previous Kv1 studies in rat layer 2/3 PNs from somatosensory cortex indicated that α-dendrotoxin (DTX)-sensitive Kv1 currents comprised ~20% of the whole cell Kv current, with persistent Kv1 currents found in all PNs. The DTX-sensitive current was relatively insensitive to holding potential, consistent with a half-inactivation voltage of approximately −50 mV. A subset of layer 2/3 cells also had a rapidly inactivating Kv1 component (Guan et al. 2006). Single-cell RT-PCR, immunocytochemistry, and recordings with Kv1-selective toxins indicated expression of Kv1.1, Kv1.2, Kv1.3, and Kv1.4, with most cells expressing two or more of these α-subunits (Guan et al. 2006). In layer 2/3 PNs, Kv1 currents activated at voltages subthreshold for APs and thus regulated AP voltage threshold, rheobase, and the rate and gain [frequency-current (*f-I*) slope] of repetitive firing (Guan et al. 2007b). In the present study, we used voltage-clamp recordings from somatic outside-out macropatches to determine the amplitude and biophysical properties of Kv1 currents in *etv1* and *glt* PNs. We then used whole cell current-clamp recordings to test the hypotheses that Kv1 channels differentially regulate the AP [voltage threshold, repolarization rate of change of voltage (dV/dt), and width], rheobase, and repetitive firing in these two PN types.

METHODS

All procedures were performed in strict accordance with the *Guide for the Care and Use of Laboratory Animals* of the National Institutes of Health (NIH) and were approved by the University of Tennessee Health Science Center Institutional Animal Care and Use Committee. Mice were maintained under standard light-dark cycles and allowed to feed and drink ad libitum.

We studied layer 5 PNs from two bacterial artificial chromosome (BAC) lines of mice, each of which express EGFP in different subpopulations of layer 5 PNs (Gong et al. 2002, 2003, 2007; Groh et al. 2010; Guan et al. 2015). In the somatosensory cortex of Tg(*Etv1* EGFP)BZ192Gsat/Mmucd (*etv1*) mice, EGFP is primarily expressed in PNs from superficial layer 5 (Groh et al. 2010; Guan et al. 2015). In somatosensory cortex of Tg(*Glt25d2*-EGFP)BN20Gsat/Mmnc (*Glt*) mice, *glt*-EGFP is primarily expressed in a subset of deep layer 5 PNs (Groh et al. 2010; Guan et al. 2015). We maintain breeding colonies of these mice (Swiss-Webster background), which were originally obtained from the Mutant Mouse Regional Resource Centers of the GENSAT project. For the original description of these BAC lines, see Gong et al. (2007) and Doyle et al. (2008). A detailed characterization is found in Groh et al. (2010). We previously characterized the laminar location and firing properties of PNs in these two mouse lines (Bishop et al. 2015; Guan et al. 2015).

Glt and etv1 brain slices. Recordings were performed on juvenile male and female mice from 3 to 6 wk of age. Mice were anesthetized with isoflurane until they were areflexive to tail pinch. Briefly, the mouse was placed into a sealed plastic container into which gauze soaked with isoflurane was placed under a fiberglass screen floor. After anesthesia, the animal was decapitated and the brain was removed and dropped into ice-cold cutting solution bubbled with O_2 for ~60 s. This solution contained the following (in mM): 250 sucrose, 2.5 KCl, 1 NaH_2PO_4, 11 glucose, 4 $MgSO_4$, 0.1 $CaCl_2$, 0.4 ascorbate, 0.6 sodium pyruvate, and 15 HEPES, pH 7.3–7.4, 300 mosM. The brain was then sliced into 300-μm-thick coronal sections using a vibrating tissue slicer (Vibroslice; Campden Instruments). We used a recirculating bath system with a peristaltic pump (Gilson Minipuls 3) controlling both the inflow and the outflow of carbogenated artificial cerebrospinal fluid (aCSF).

Current-clamp recordings in brain slices. Slices were placed in a recording chamber on the stage of an Olympus BX50WI upright microscope and bathed in aCSF bubbled with 95% O_2-5% CO_2 at 2 ml/min and heated with an in-line heater (Warner Instruments) to 33 ± 1°C. The aCSF contained the following (in mM): 125 NaCl, 3 KCl, 2 $CaCl_2$, 2 $MgCl_2$, 1.25 NaH_2PO_4, 26 $NaHCO_3$, and 20 glucose (pH 7.4, 310 mosM). Pharmacological agents were added directly to the aCSF. PNs in layer 5 were visualized with infrared differential interference contrast (IR-DIC) video microscopy (Dodt and Zieglgänsberger 1990; Stuart et al. 1993) using a ×40 (0.8 numerical aperture) Olympus water-immersion objective and an IR-sensitive camera (Olympus OLY-150 or DAGE-MTI). *Etv1* or *glt* PNs were visually identified by the presence of EGFP epifluorescence using an FITC filter. Recordings were directed within the main band of EGFP+ cells in layer 5 in each slice. We switched between IR-DIC and epifluorescence to determine cell type and to obtain a gigaohm seal. Electrode position was controlled with Sutter Instruments (Novato CA) or Luigs-Neumann (Ratingen, Germany) manipulators and controllers. Whole cell patch-clamp recordings were acquired using an Axon Multiclamp 700A and 700B amplifiers (Molecular Devices, Sunnyvale, CA) and pCLAMP 9 or 10 software.

We recorded with borosilicate electrodes (model GC150TF; Warner Instruments, Hamden, CT) that were produced with a horizontal electrode puller (Flaming-Brown P-87; Sutter Instruments, Novato CA). Electrode resistances were 1.5–4 MΩ in the bath. For current-clamp recordings, electrodes were filled with an internal solution containing the following (in mM): 130.5 $KMeSO_4$, 10 KCl, 7.5 NaCl, 2 $MgCl_2$, 10 HEPES, 2 ATP, 0.2 GTP, and 0.1 EGTA (adjusted to pH 7.25 with 1 N KOH, ~290 mosM). Data were only collected from cells forming a seal of 1 GΩ or tighter. For current-clamp, cells also had overshooting APs with amplitude >60 mV and fired repetitively. All reported voltages were corrected by subtracting the measured liquid junction potential (8 mV). We compensated for electrode capacitance, and bridge balance was carefully monitored. Recordings were terminated in cells where access resistance was >20 MΩ or increased dramatically during the recording. Data were digitized at 20 KHz and filtered at 10 kHz.

All slice current-clamp recordings were in the presence of 6,7-dinitroquinoxaline-2,3-dione (DNQX; 20 μM) to block α-amino-3-hydroxy-5-methyl-4-isoxazoleproipionic acid (AMPA) receptors, D-(−)-2-amino-5-phosphonopentanoic acid (D-AP5; 50 μM) to block *N*-methyl-D-aspartate (NMDA) receptors, and picrotoxin (100 μM) to block γ-aminobutyric acid type A ($GABA_A$) receptors to minimize

the effects of the pharmacological agents on fast synaptic transmission. Potassium channel blockers were added directly to the aCSF. Most reagents were purchased from Sigma-Aldrich (St. Louis, MO). In addition, DTX and margatoxin (MTX) were purchased from Alomone Labs (Jerusalem, Israel). DNQX, D-AP5, and picrotoxin were purchased from Tocris Bioscience (Ellsville, MO).

Voltage-clamp recordings. To obtain accurate biophysical measurements of outward K^+ currents, we used outside-out macropatches that were formed after break-in to whole cell mode by withdrawing the pipette without additional suction. The patch capacitance was 1–4 pF and series resistance was 5–9 MΩ. For outside-out voltage-clamp recordings, electrodes were filled with an internal solution containing the following (in mM): 135 $KMeSO_4$, 2 $MgCl_2$, 10 HEPES, 2 ATP, 0.2 GTP, and 0.25 leupeptin (pH adjusted to 7.2 with 1 N KOH, ~290 mosM). EGTA (5 mM) was added to the intracellular solution to prevent activation of Ca^{2+}-dependent conductances. Tetrodotoxin (0.5 μM) was added to the bath to block Na^+ channels and Cd^{2+} (200 μM) to block Ca^{2+} channels. Kv1 channel blockers were dissolved directly into aCSF containing 0.1% bovine serum albumin (BSA).

For voltage-clamp recordings, the data were digitized at 10 kHz and filtered at 4 kHz. To determine steady-state voltage dependence, a family of 500- or 1,000-ms voltage steps was made from a holding potential of −75 mV to voltages between −50 and +40 mV in 10-mV increments (20 s between sweeps). This protocol was run in control solution without channel blockers and repeated after application of Kv1 blockers. The blocker-sensitive current was obtained by subtracting traces in blocker from control traces. Current at 500 ms was converted to conductance by dividing current by driving force ($E - E_K$, where E_K, the equilibrium potential of K^+, was calculated as −102 mV from the internal and external K^+ concentrations). Conductance was normalized by the maximum conductance (G_{max}), and normalized conductance was plotted as a function of test voltage. These data were then fit with a single Boltzmann relationship as follows:

$$G = G_{max}/\{1 + \exp[(V_{50} - V)V_{slope}]\}, \quad (1)$$

where G is the calculated conductance, V_{50} is the half-activation voltage, V is the step potential, and V_{slope} is the slope factor for activation. Data from both *etv1* and *glt* PNs were well fit by a single Boltzmann equation.

Steady-state inactivation was studied by comparing the response to a test step to +10 mV (500 ms) immediately following 5-s prepulses to voltages between −100 and −20 mV (20 s between steps). Current amplitudes (I) were normalized to the largest response (I_{max}) and plotted vs. prepulse voltage. These data were fit with a single Boltzmann relationship of the following form:

$$I/I_{max} = 1/\{1 + \exp[(V - V_{1/2})V_c]\}, \quad (2)$$

where $V_{1/2}$ is the half-inactivation voltage and V_c is the slope factor for inactivation.

To compare activation and inactivation kinetics between cell types, we fit the rising and decay phases of currents, each with a single exponential (*Eq. 2*). A 500- or 1,000-ms step from −75 to various potentials between −50 and +40 mV was used to elicit currents. Blocker-sensitive currents were used to fit the following activation-inactivation equation:

$$I(t) = I_0[1 - \exp(-t/\tau_0)]^2 \cdot [\exp(t/\tau_1) + C], \quad (3)$$

where $I(t)$ represents the blocker-sensitive current, I_0 represents the maximum current, τ_0 is the activation time constant, τ_1 is the inactivation time constant, and C is a constant.

Statistics. Prism (GraphPad, La Jolla, CA) software was used to perform statistical tests on the data. Student's *t*-test was used to compare sample population data, and summary data are means ± SE unless otherwise stated. Paired *t*-tests were used to compare control vs. drug effects. We used a one-way ANOVA to compare multiple experimental groups, with post hoc Tukey's multiple comparison tests to determine which individual means differed. For all tests, P values <0.05 were considered significantly different. Sample population data are represented as histograms of mean ± SE or scatter plots. Chi square tests were used to determine differences in the distributions of response types.

RESULTS

Voltage-clamp recordings. We made recordings with outside-out macropatches taken from somatic membranes of PNs identified as EGFP+ in slices from *etv1* or *glt* mice. The macropatches provide excellent voltage control and allow recordings in slices at 33 ± 1°C. Our conclusions are thus restricted to channels expressed on the soma. In rat layer 2/3 PNs, we previously determined the presence of several Kv1 α-subunits in a single PN (Guan et al. 2006) and that 100 nM DTX was a saturating dose (Guan et al. 2006). We confirmed in the present study that 200–300 nM DTX blocked no more current than 100 nM DTX in mouse layer 5 PNs ($n = 4$ cells; data not shown). DTX has been shown to selectively block channels containing Kv1.1, Kv1.2, or Kv1.6 α-subunits (Harvey and Robertson 2004). At low nanomolar doses, MTX blocks channels containing Kv1.3 α-subunits, although it also blocks Kv1.2 subunits (Bartok et al. 2014). We found that MTX blocked Kv current in layer 5 PNs with an EC_{50} of ~3 nM ($n = 7$; data not shown) and that 30–40 nM MTX was a saturating dose.

To test whether MTX blocked current that was not blocked by DTX, we isolated currents sensitive to 100 nM DTX, 20–40 nM MTX, or DTX plus MTX (Fig. 1, *A–C*). The examples show currents from a *glt* PN in control solution and in the presence of 100 nM DTX plus 30 nM MTX, and the putative Kv1-mediated current, i.e., the subtracted traces [control – (DTX+MTX)]. Kv1-mediated currents (DTX+MTX sensitive) were similar in amplitude in *glt* and *etv1* PNs for both peak and steady-state (500 ms) currents. For peak current, about 25–30% of current was blocked by DTX alone or MTX alone; this %block did not differ significantly between PN types. The combined DTX plus MTX blocked ~35% of peak current in both PN types (Fig. 1, *D* and *E*). At steady state, a similar pattern emerged: 20–25% block by DTX, ~15% block by MTX, and 25–30% by the combined toxins. Again there were no significant differences between PN types or between toxins. These data suggest that most Kv1.3 subunits may be expressed in the same heteromeric channels with Kv1.1, Kv1.2, and/or Kv1.6 (see also Miller et al. 2008).

Consistent with the relatively depolarized half-inactivation voltage for the current sensitive to Kv1 blockers (see Fig. 5), this current was relatively insensitive to holding potential. In 8 *etv1* and 9 *glt* PNs, we measured the amplitude of the whole current and the toxin-sensitive and toxin-resistant components from a holding potential of −75 mV, with or without a 1-s prepulse to −100 mV. Whereas the whole current and toxin-resistant components were significantly larger after the −100-mV prepulse, the amplitude of the current sensitive to Kv1 blockers was unchanged (data not shown).

We next assessed the biophysical properties of Kv1-mediated currents in *etv1* and *glt* PNs (Fig. 2, *A–F*). First, we measured τ values for currents in response to a test step from −75 to +10 mV. We observed considerable variability in the amount and rate of inactivation of DTX-, MTX-, or DTX+

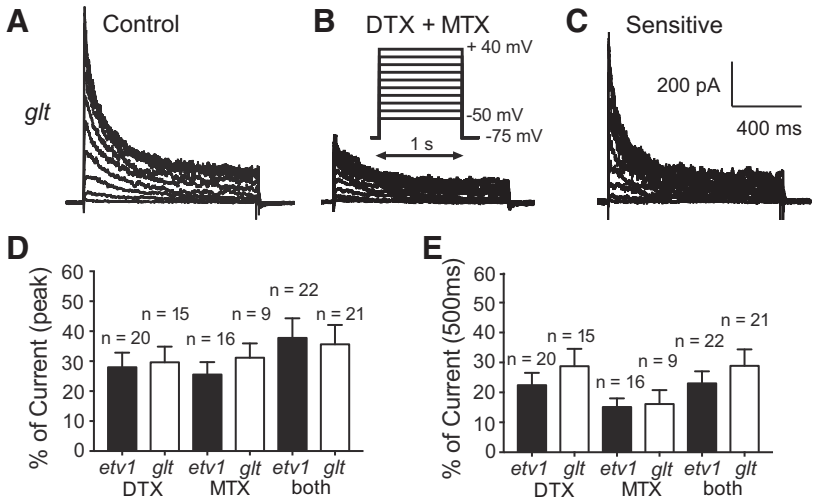

Fig. 1. Kv1-mediated currents in *etv1* and *glt* pyramidal neurons. *A*: family of current traces from *glt* cell in control solution in response to protocol shown as *inset* in *B* (1-s steps). *B*: current traces from the same cell as in *A*, except in the presence of 100 nM α-dendrotoxin (DTX) + 30 nM margatoxin (MTX). *Inset*: voltage protocol for *A–C*. *C*: subtracted records (control − DTX+MTX) to show putative Kv1-mediated current. *Inset*: scale bars for *A–C*. *D*: summary data (means ± SE) for %block at peak current at +10 mV by 100 nM DTX, 30 nM MTX, or both toxins combined in *etv1* and *glt* cells. *E*: summary data (means ± SE) for %block at steady state (500 ms, +10 mV) by 100 nM DTX, 30 nM MTX, or both toxins combined in e*tv1* and *glt* cells.

MTX-sensitive currents in patches from both *etv1* and *glt* PNs (Fig. 2). This variation was similar within each cell type and for all toxin-sensitive currents.

Toxin-sensitive currents in most mouse layer 5 PNs were well fit by a single exponential for activation and a single exponential for inactivation (plus a remaining, persistent component: *Eq 3*: see METHODS). The currents activated rapidly (τ ~1 ms: second-order fit), and this did not differ significantly between PN types or toxins (Fig. 2*G*), except in *glt* PNs, where DTX-sensitive current activated significantly more slowly than MTX-sensitive current ($P < 0.04$). Most patches had inactivating and persistent components. At +10 mV, the value for *C* (the persistent component in *Eq. 3*) was 0.42 ± 0.09 for *etv1* and 0.47 ± 0.15 for *glt* PNs (not significantly different). The inactivation time constants were ~100–300 ms at +10 mV and generally did not differ significantly between PN types or toxin-sensitive currents (Fig. 2*H*). The exception was that DTX-sensitive currents in *etv1* PNs inactivated faster than MTX-sensitive currents ($P < 0.04$). The overall %inactivation (peak to 500 ms) was between 65% and 80% at + 10 mV. The only significant difference for %inactivation was in *etv1* cells, where MTX-sensitive current inactivated more than DTX-sensitive current ($P < 0.006$: Fig. 2*I*).

Figure 3, *A and B*, shows the time constants for activation and inactivation at each of the voltages tested in the steady-state activation and inactivation protocols (shown in Figs. 4 and 5). The currents in response to steps from −30 to +40 mV were fit with *Eq. 3*. The activation and inactivation time constants were not significantly different in *etv1* vs. *glt* PNs. At −40 mV, there was no transient component to the current in *etv1* PNs (approximately no inactivation over the 500-ms step).

We examined the voltage dependence of steady-state activation in *etv1* and *glt* cells (Fig. 4). The current sensitive to Kv1 blockers activated in the subthreshold voltage range, beginning at approximately −60 mV (Fig. 4, *A and B*). The half-activation voltage and slope did not differ significantly between *etv1* and *glt* PNs or between toxins (DTX, MTX, or DTX+MTX; Fig. 4, *D* and *E*). We therefore combined data for all Kv1 blockers to compare steady-state activation voltage and slope. We found no significant differences between *etv1* and *glt* (Fig. 4, *C* and *F*). Collectively, our voltage-clamp data suggest minimal biophysical differences between DTX- and MTX-sensitive currents or between Kv1 currents in *etv1* and *glt* PNs.

The voltage dependence of steady-state inactivation was examined in 9 *etv1* and 10 *glt* PNs by measuring the response to a 500-ms test step to +10 mV immediately following 5-s

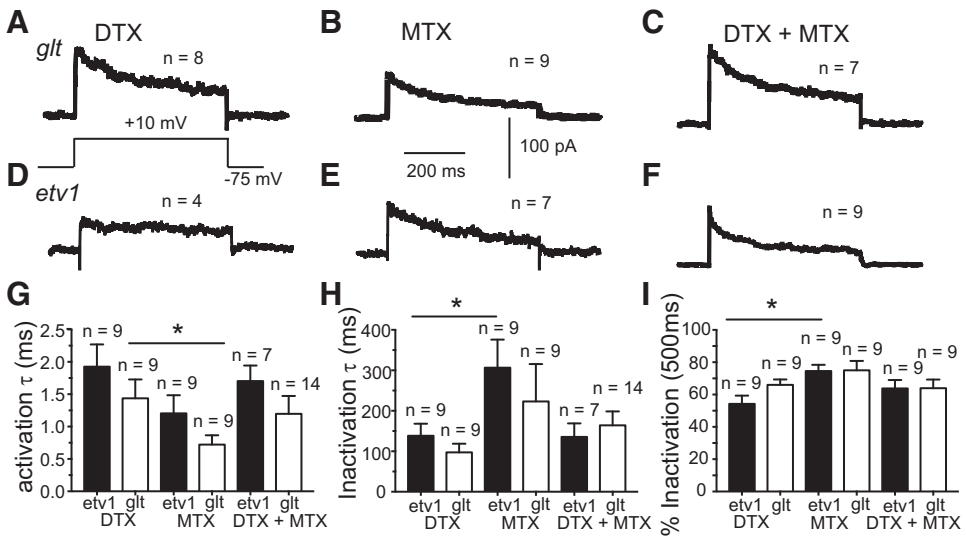

Fig. 2. Outside-out macropatch currents and their kinetics. *A–F*: representative current traces of average currents sensitive to α-dendrotoxin (DTX; 100 nM), margatoxin (MTX; 20–40 nM), or DTX+MTX in *glt* (*A–C*) and *etv1* (*D–F*) pyramidal neurons (PNs). The protocol shown in *A* applies to *A–F*. *G*: summary data (means ± SE) for activation time constant (τ) at +10 mV. There were no significant differences between PN types. In *glt* PNs, MTX-sensitive currents activated more rapidly than DTX-sensitive currents ($^*P < 0.05$). *H*: summary data (means ± SE) for inactivation τ (at +10 mV). There were no significant differences between PN types. In *etv1* PNs, DTX-sensitive currents inactivated more rapidly than MTX-sensitive currents ($^*P < 0.05$). *I*: summary data (means ± SE) for %inactivation (at +10 mV). There were no significant differences between PN types. In *etv1* PNs, MTX-sensitive currents inactivated more than DTX-sensitive currents ($^*P < 0.05$).

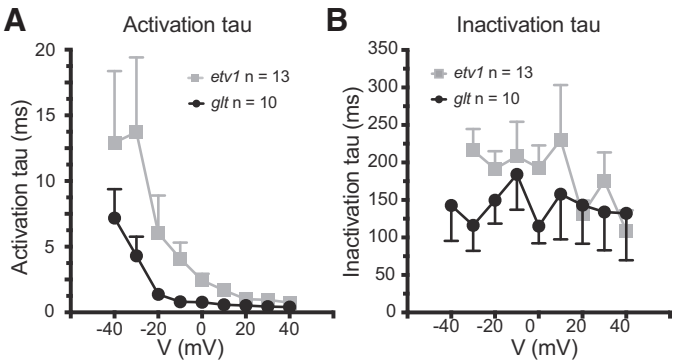

Fig. 3. Activation and inactivation time constants (tau). The rise (activation) and decay (inactivation) for the Kv1 blocker-sensitive current were fitted at several voltages (*V*) using the activation protocol shown in Fig. 4 (for fitting procedure, see *Eq. 3* in text). *A*: activation tau values were not significantly different between *etv1* and *glt* pyramidal neurons (PNs). *B*: inactivation tau values were not significantly different between *etv1* and *glt* PNs and showed little voltage dependence. Data are means ± SE.

prepulses to various potentials between −100 and −20 mV from the holding potential of −75 mV (Fig. 5*A*). We waited 20 s between each prepulse + test pulse. The test currents were normalized by the maximum current and plotted vs. test voltage (Fig. 5*B*). A single Boltzmann fit (*Eq. 2*) revealed half-inactivation voltages of −53.8 ± 1.8 mV for *etv1* and −51 ± 1.7 mV for *glt* (no significant difference; Fig. 5*C*). The corresponding slopes were 5.1 ± 0.8 mV for *etv1* and −6.1 ± 0.9 mV for *glt* (no significant difference: Fig. 5*D*).

Current-clamp recordings. We next tested functional roles of Kv1 channels in *etv1* and *glt* PNs using whole cell current-clamp recordings in acute brain slices (at 33 ± 1°C). All recordings were in the presence of blockers of fast synaptic transmission, and we used a recirculating bath to apply the Kv1 blocking toxins (100 nM DTX, 10–30 nM MTX, or the combination). Table 1 indicates basic electrical properties of the *etv1* and *glt* PNs, which were similar to our previous findings for these cell types (Guan et al. 2015; Pathak et al. 2016). Consistent with our voltage-clamp experiments, we found no differences for AP parameters, rheobase (the minimum amount of current required to elicit an AP with a prolonged current injection), or *f-I* relationships among DTX, MTX, or DTX+MTX, so we combined the data for all Kv1 blockers and compared these data with that for their respective controls. On the basis of the rapid activation kinetics and subthreshold activation range of Kv1-mediated currents, we predicted that block of Kv1 channels in layer 5 PNs would regulate rheobase, voltage threshold for an AP, and repolarization of the AP. We also hypothesized that Kv1 channels regulate repetitive firing behavior (delay to first AP, firing rate, *f-I* slope) and tested whether the functional roles of Kv1 channels differ in a PN type-specific manner.

Individual APs were elicited with 5-ms current injections (Fig. 6), and we compared AP properties before and after application of Kv1 blockers. Voltage threshold was measured as the voltage corresponding to the rapid upward deflection in plots of d*V*/d*t* vs. membrane potential (V_m). The voltage threshold for an AP was significantly shifted to more negative potentials by Kv1 blockers in both PN types (Fig. 6*C*; $P < 0.007$ for *etv1*, $P < 0.001$ for *glt*). Consistent with our previous findings (Pathak et al. 2016), Kv1 block increased AP half-width in *etv1* but not *glt* PNs (Fig. 6*D*; $P < 0.0008$ for *etv1*, $P < 0.09$ for *glt*). The AP broadening was due to reduced AP repolarization as indicated by significantly reduced d*V*/d*t* for repolarization in *etv1* PNs after Kv1 block (117 ± 6 vs. 130 ± 6 V/s in control, $n = 43$, $P < 0.005$). No significant changes in repolarization d*V*/d*t* were observed in *glt* PNs (all toxins combined: 184 ± 7 control vs. 186 ± 9, $n = 50$, $P < 0.68$).

Consistent with Kv1 activation at subthreshold voltages, rheobase was significantly reduced in both *etv1* and *glt* PNs by

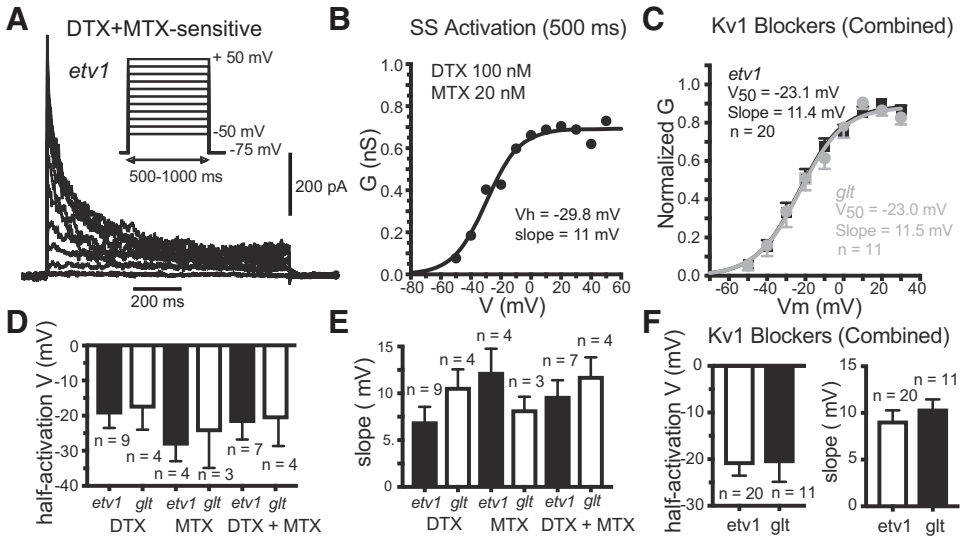

Fig. 4. Steady-state activation of Kv1-mediated currents. *A*: current traces sensitive to 100 nM α-dendrotoxin (DTX) + 20 nM margatoxin (MTX) from outside-out macropatch from an *etv1* pyramidal neuron (PN). *Inset*: voltage protocol (500- to 1,000-ms steps). *B*: steady-state (at 500 ms) activation curve for cell in *A*. *C*: summary activation curves (at 500 ms; means ± SE) for current sensitive to Kv1 blockers (combined data: DTX, MTX, and DTX+MTX) for *etv1* (black) and *glt* PNs (gray). *D*: summary data (means ± SE) for half-activation voltage in *etv1* and *glt* PNs for current sensitive to 100 nM DTX, 20–40 nM MTX, or their combination (DTX+MTX). There were no significant differences. *E*: summary data (means ± SE) for activation slope for current sensitive to 100 nM DTX, 30–40 nM MTX, or their combination (DTX+MTX). There were no significant differences. *F*: summary data for half-activation voltage and slope for *etv1* vs. *glt* PNs (all Kv1 blockers combined: DTX, MTX, and DTX+MTX). There were no significant differences. *G*, conductance; SS, steady state; *V*, voltage; V_m, membrane potential.

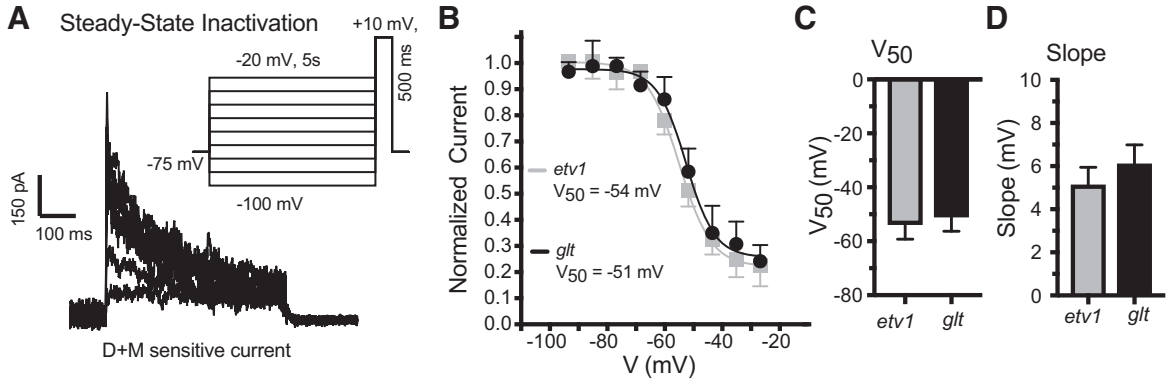

Fig. 5. Steady-state inactivation. The steady-state inactivation of currents sensitive to 100 nM α-dendrotoxin (DTX) + 30 nM margatoxin (MTX) was compared in outside-out macropatch recordings from 9 *etv1* and 10 *glt* pyramidal neurons (PNs). From a holding potential of −75 mV, the current was inactivated with 5-s steps to voltages between −100 and −20 mV and then measured from a test step to +10 mV (20 s between each prepulse + test step). *A*: representative traces from a patch from a *glt* PN. *Inset*: voltage protocol. *B*: plot of normalized current vs. prepulse voltage (*V*) for patches from *etv1* (black) and *glt* (gray) PNs (means ± SE). There were no significant differences between cell types. *C*: histograms (means ± SE) comparing *etv1* and *glt* for the half-inactivation voltage (V_{50}). There were no significant differences between cell types. For *etv1*, V_{50} was −53.8 ± 1.8 mV, and for *glt* it was −51 ± 1.7 mV. *D*: histograms (means ± SE) comparing *etv1* and *glt* for half-inactivation slope. For *etv1*, the slope was 5.1 ± 0.8 mV, and for *glt* it was 6.1 ± 0.9 mV. There were no significant differences between cell types.

Kv1 blockers (Fig. 7, *A* and *B*; $P < 0.0001$ for *etv1*, $P < 0.0001$ for *glt*). For the combined data (all toxins), the rheobase decrease was 34 ± 3% in *etv1* ($n = 64$) and 28 ± 3% in *glt* ($n = 76$). The latency to the first AP in response to a low-amplitude, long current injection (200 pA, 500 ms) was also significantly reduced by Kv1 blockers (all data combined; Fig. 7*C*). Latency was decreased by 43 ± 6% in *etv1* ($n = 38$) and 53 ± 4% in *glt* ($n = 42$).

Groh et al. (2010) reported that in control solutions, *glt* PNs were more likely to fire with an initial doublet in response to suprathreshold current injections than *etv1* PNs. If a doublet is defined as the first interspike-interval (ISI) being much shorter than subsequent ISIs, our initial experiments suggested that the presence of an onset doublet depended on the stimulus current, with higher currents being more likely to elicit a doublet (Fig. 8, *A* and *B*). We looked at the relationship between the first, second, and third ISIs and injected current for *etv1* ($n = 37$) and *glt* ($n = 39$) PNs. In the examples shown in Fig. 8, *A–C*, it can be seen that above 200–300 pA, the first ISI was shortened with increased current much more than subsequent ISIs (providing an alternative definition for an onset doublet). These relationships held for the population of *etv1* (Fig. 8*G*) and *glt* (Fig. 8*H*). With high enough currents (400–600 pA), all PNs fire with an onset doublet defined in this manner (Fig. 8, *F* and *I*). Kv1 blockers had similar effects on both *etv1* and *glt* PN. Kv1 block shifted the relationship to the left, resulting in less current being required to elicit an onset doublet (Fig. 8, *C* and *F–I*).

Glt PNs displayed two firing behaviors not observed in *etv1* PNs. In a small number of *glt* PNs (8/78, 10.2%) an onset burst of 3–5 APs riding on a slow depolarization was observed. This response is similar to burst firing as initially described by the Prince laboratory (Connors et al. 1982), so we referred to this firing as an onset burst (Fig. 9*A*). In the presence of Kv1 blockers, an additional 6 cells fired with an onset burst (total = 14/78, 17.9%). In contrast to our findings in neocortical PNs, significantly increased burst firing (Metz et al. 2007) and dendritic spiking (Golding et al. 1999) were previously observed in a different type of PN after DTX (CA1 PNs).

As previously reported for PNs in layer 5 of rat motor cortex (Miller et al. 2008), a small number of *glt* PNs from layer 5 of mouse somatosensory cortex showed acceleration of firing rate during a 1- to 2-s current injection (Fig. 9, *B* and *C*). Whereas no *etv1* PNs exhibited this acceleration, firing in 4 of 52 *glt* PNs (8%) accelerated during a 2-s current injection. Figure 9*C* shows plots of instantaneous firing frequency (1/ISI) vs. time for a *glt* PN that showed acceleration in control solution (rising curve with time) that was changed to higher rate firing with SFA after MTX. In Kv1 blockers, acceleration was lost in three of four cells (2 in MTX, 1 in DTX+MTX; the cell that still accelerated was in DTX).

We next examined effects of Kv1-mediated currents on repetitive firing of mouse layer 5 PNs. The majority of *etv1* and *glt* PNs fired in a regular spiking pattern. As an initial test for effects of Kv1 block on firing rate, we compared firing in response to a test current step adjusted to elicit firing at ~10 Hz for 2 s in the control solution. This same current amplitude was then applied after application of Kv1 blockers. The pattern of response was similar for DTX, MTX, or DTX+MTX, so the data were combined. Kv1 block resulted in increased firing rate in both *etv1* and *glt* PNs (Fig. 10, *A* and *B*; $P < 0.0001$ for *etv1*, $P < 0.0001$ for *glt*).

We then generated average *f-I* curves for firing in response to a family of 2-s current injections in both *etv1* and *glt* PNs.

Table 1. *Basic properties of etv1 vs. glt pyramidal neurons*

	RMP, mV	R_{in}, MΩ	AP, mV	APHW, ms	Rheobase, pA
etv1	−74 ± 1 (46)	109 ± 7 (45)	95 ± 2 (44)	0.77 ± 0.03 (44)	135 ± 10 (42)
glt	−72 ± 1 (48)	88 ± 6* (49)	98 ± 1 (50)	0.59 ± 0.02* (50)	125 ± 13 (42)

Data are means ± SE (no. of cells). RMP, resting membrane potential; R_{in}, steady-state input resistance; AP, action potential amplitude; APHW, action potential width at half-amplitude. *$P < 0.05$, significantly different from *etv1*.

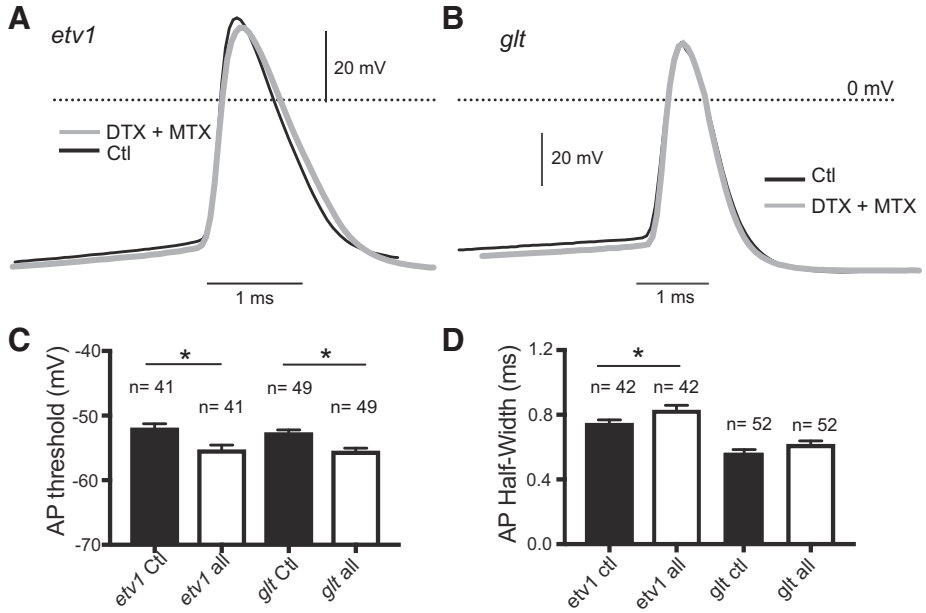

Fig. 6. Effects of Kv1 channels on the action potential (AP). *A*: representative traces for single APs elicited by a 5-ms suprathreshold current injection in a *etv1* pyramidal neuron (PN) in control solution (Ctl) and in the presence of 100 nM α-dendrotoxin (DTX) + 30 nM margatoxin (MTX). Note slightly hyperpolarized AP voltage threshold and broadening of the AP. *B*: similar traces for *glt* PN. Note narrower AP compared with *etv1* PN in *A* and shift in threshold but no change in AP width in DTX+MTX. *C*: summary histograms (means ± SE) for AP voltage threshold for e*tv1* and *glt* PNs in Ctl vs. combined data for DTX (100 nM), MTX (20 nM), and DTX+MTX (all). There was a significant hyperpolarization of AP threshold in both cell types (*$P < 0.05$). *D*: summary histograms (means ± SE) for AP width at half-amplitude (half-width) for *etv1* and *glt* PNs in Ctl vs. Kv1 blockers (all = combined data for DTX, MTX, and DTX+MTX). There was significant AP broadening in *etv1* PNs but not in *glt* PNs (*$P < 0.05$).

We compared the initial linear portion of the *f-I* relationship for the entire 2 s of firing. The effects on *f-I* relationships to DC differed between PN types. In both *etv1* and *glt* PNs, Kv1 blockers caused an increased initial *f-I* slope (Fig. 10, *C–E*; $P < 0.0001$ for *etv1*, $P < 0.0001$ for *glt*). However, the magnitude of this gain change was much greater in *etv1* (154 ± 21%, $n = 38$) than in *glt* (16 ± 4%; $n = 42$) PNs.

We also studied changes in firing rate over time. We quantified SFA as percent adaptation, defined as [(ISI at 2s − 3rd ISI/ISI at 2s) × 100]. We chose the third ISI to focus on slow SFA as opposed to mechanisms regulating fast adaptation during the first two ISIs (which are likely related to doublet and burst firing mechanisms). Most *etv1* PNs showed strong SFA (Fig. 11*A*; Guan et al. 2015). In contrast, most *glt* PNs showed no SFA or little SFA (Fig. 11*B*), although a few *glt* PNs showed acceleration during a 2-s firing epoch (see above). In *etv1* PNs, Kv1 block resulted in little change in SFA to small currents (or at low firing rates) and significantly reduced SFA at high currents (and high firing rates; Fig. 11*C*). The combined data for *glt* PNs show little SFA in control, and the effects of Kv1 block are similarly minimal for all currents, although SFA was only significantly higher at the lowest current (Fig. 11*C*). These results differ from our findings for DTX-sensitive currents in rat layer 2/3 PNs, where no effect on SFA was observed (Guan et al. 2007).

DISCUSSION

We studied two genetically identified PN types from layer 5 of mouse cortex to test for differences in expression of Kv1 currents and their functional roles. We first used voltage-clamp recordings and Kv1-selective peptides to determine the amplitude and biophysical properties of putative Kv1 currents in *etv1* and *glt* PNs (IT- and PT-type PNs, respectively). We then used

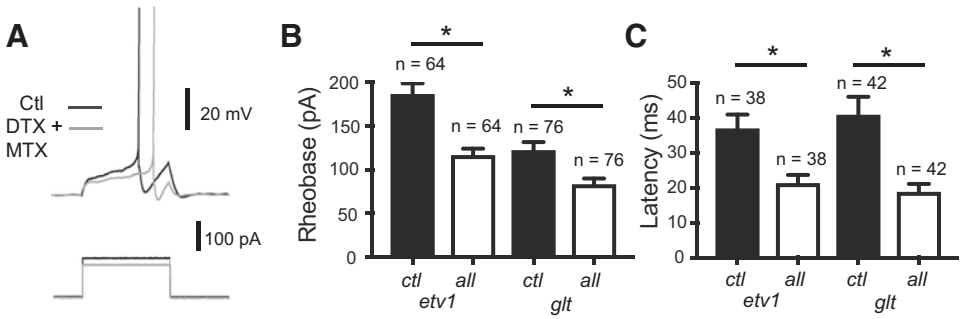

Fig. 7. Effects of Kv1 channels on rheobase and latency to the first action potential (AP). *A*: representative traces from a *glt* pyramidal neuron (PN) showing reduced current required to elicit an AP during 500-ms current injection (decreased rheobase) in the presence of 100 nM α-dendrotoxin (DTX) + 30 nM margatoxin (MTX; gray traces) and control (Ctl; black traces). *B*: summary histograms (means ± SE) showing that Kv1 blockers (all = combined data for DTX, MTX, and DTX+MTX) significantly reduced rheobase in both *etv1* and *glt* PNs (*$P < 0.05$). *C*: summary histograms (means ± SE) showing that Kv1 blockers significantly reduced latency to the first AP in response to a 200-pA, 500-ms current injection in both *etv1* and *glt* PNs (*$P < 0.05$).

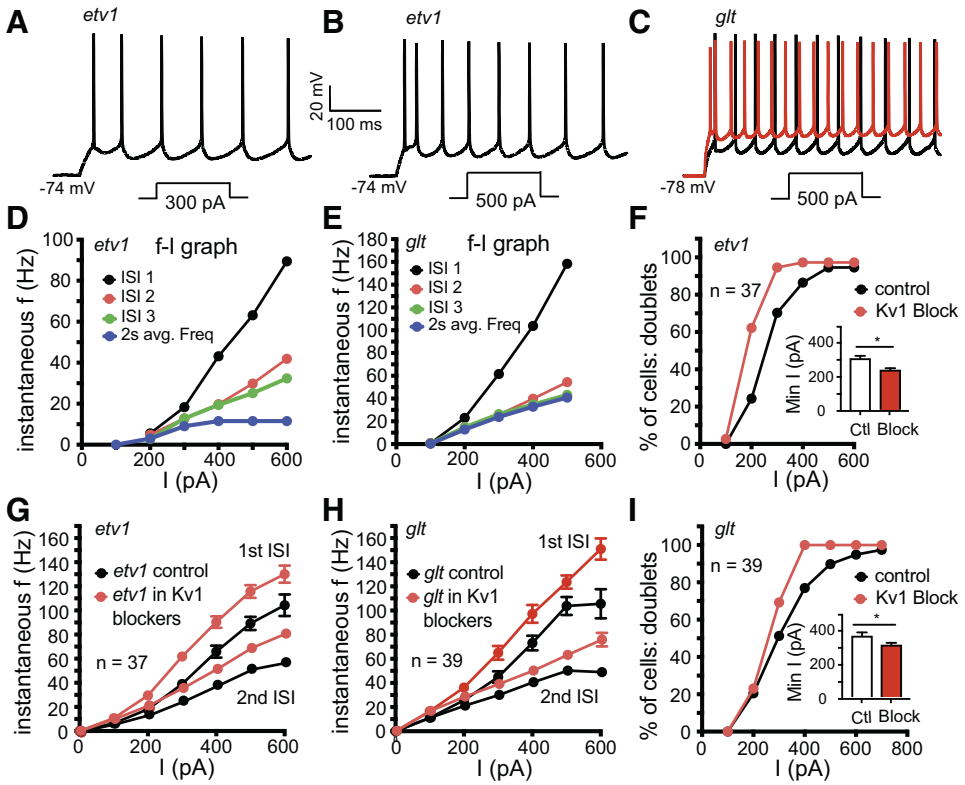

Fig. 8. Onset doublets. *A*: traces from an *etv1* pyramidal neuron (PN) showing regular spiking at onset of response to direct current (DC) injection (300 pA, 2 s) in control solution. Scale bars apply to *A–C*. *B*: traces from the same *etv1* PN in control solution in response to a larger (400 pA, 2 s) current injection. Note the initial doublet of action potentials (APs) at the onset of the response. *C*: traces from a *glt* PN showing regular spiking at the onset of a DC injection (250 pA, 2 s) in control solution (black trace). After 100 nM α-dendrotoxin (DTX) + 30 nM margatoxin (MTX; red), there was an initial doublet of APs at the onset of the current step. *D*: plot of instantaneous firing frequency [*f*; 1/interspike interval (ISI)] vs. injected current (*I*) for the *etv1* PN from *A* and *B*. Plotted are the first 3 ISIs as well as average firing over the entire 2-s epoch. Note the sharp deviation of the curve for the first ISI vs. the others at currents >300 pA. This deviation was diagnostic for the presence of an initial doublet and served as our working criteria for the presence of a doublet. *E*: similar plot for a *glt* PN. As in the *etv1* PN, there was a sharp deviation of the first ISI curve above 200 pA, reflecting onset doublet in response to currents >200 pA. *F*: plot of the percentage of cells showing an onset burst at a given level of injected current using the criteria shown in *D* and *E*. In control solution (black), virtually all cells could fire with an onset burst in response to currents >500 pA. After Kv1 block (red), the curve was shifted leftward, indicating a reduction in the current required to initiate an onset doublet. *Inset*: histogram (means ± SE) indicating that Kv1 block results in a significant reduction in the minimal current to elicit an onset doublet (*$P <$ 0.05). *G*: plot of instantaneous firing frequency (1/ISI; means ± SE) for the first vs. the second ISI vs. the injected current for a population of 37 *etv1* PNs in control (black) and Kv1 blockers (red). Kv1 block increased the frequency for both the first and second intervals but had a greater effect on the first interval, resulting in deviation from the first vs. second ISI at lower currents. *H*: similar plot and similar effects of Kv1 block for a population of 39 *glt* PNs. *I*: plot of the percentage of cells showing an onset burst at a given level of injected current using the criteria shown in *D* and *E*. In control solution (black), virtually all cells could fire with an onset burst in response to currents >500 pA. After Kv1 block (red), the curve was shifted leftward. This indicates a reduction in the current required to initiate an onset doublet. *Inset*: histogram (means ± SE) indicating that Kv1 block results in a significant reduction in the minimal current to elicit an onset doublet in *glt* PNs (*$P < 0.05$).

current-clamp recordings and Kv1-specific peptides to test the hypothesis that Kv1 channels differentially regulate AP voltage threshold, repolarization rate, and width, as well as rheobase, latency to the first AP, and repetitive firing in these two PN types. DTX-, MTX-, and DTX+MTX-sensitive currents were of similar size in both cell types. Similarly, only minor biophysical differences were observed between cell types or between currents sensitive to different toxins. Despite similar Kv1 currents, Kv1 block had differential effects on single APs and repetitive firing in the two cell types. In both PN types, Kv1 currents regulated AP voltage threshold, but AP width and rate of repolarization were only affected in *etv1* PNs. Kv1 channels regulate rheobase, onset doublets, and firing rate similarly in both cell types, but *f-I* slope and *f-t* relationships were more sensitive to Kv1 block in *etv1* PNs.

Kv1 expression. We previously showed that individual layer 2/3 PNs from rat neocortex express multiple Kv1 α-subunits, localized to somatodendritic as well as axonal cell compartments (Guan et al. 2006). All cells expressed a current sensitive to DTX (blocks channels containing Kv1.1, Kv1.2, or Kv1.6 α-subunits; Harvey and Robertson 2004). Similar currents have been observed in many cell types, although there is variation in their biophysical properties (Coetzee et al. 1999), including large layer 5 PNs (Bekkers 2000a, 2000b; Bekkers and Delaney 2001; Korngreen and Sakmann 2000), mixed populations of neocortical PNs (Dong and White 2003; Foehring and Surmeier 1993; Locke and Nerbonne 1997; Zhou and Hablitz 1996), and hippocampal PNs (Bossu et al. 1996; Chen and Johnston 2004; Halliwell et al. 1986; Wu and Barish 1992).

Kv1 subunits can form heteromultimeric channels in vitro (Heinemann et al. 1996; Po et al. 1993; Rettig et al. 1994; Salkoff et al. 1992). Kv1.1 and Kv1.2 are the most abundant subtypes in mammalian brains, and they have been detected in various combinations with Kv1.3, Kv1.4, and Kv1.6 by coimmunoprecipitation (Coleman et al. 1999; Rhodes et al. 1997;

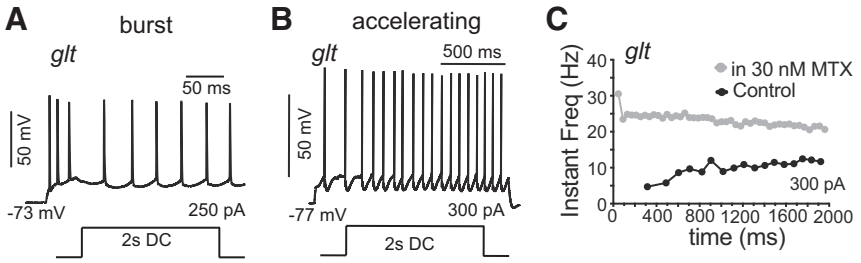

Fig. 9. Onset burst firing and acceleration during firing in *glt* pyramidal neurons (PNs). *A*: trace from a *glt* PN firing in response to a 2-s direct current (DC) injection (250 pA). There is an initial burst of 3 action potentials riding on a slow depolarization at the onset of the cell's response. In control solutions, 8/83 *glt* PNs fired with an onset burst (and no *etv1* PNs). *B*: trace from a different *glt* PN that exhibited firing that accelerated in rate during a 2-s DC injection. This pattern was observed in 4/52 *glt* PNs tested (and no *etv1* PNs). *C*: plot of instantaneous frequency [Instant Freq; 1/interspike interval (ISI)] vs. time for the *glt* PN in *B*, showing acceleration (increased frequency with time) during the 2-s firing in control solution (black). In 30 nM margatoxin (MTX; gray), the cell fired faster and acceleration was replaced with spike frequency adaptation (SFA). In 3 of 4 *glt* PNs that showed acceleration in control solutions, the acceleration was lost after Kv1 block.

Scott et al. 1994; Shamotienko et al. 1997; Wang et al. 1993, 1994). Furthermore, coimmunoprecipitation revealed in vivo associations of Kv1.2 with Kv1.4 (Sheng et al. 1994), Kv1.1 with Kv1.2 (Wang et al. 1993), and Kv1.2 with Kv1.3 (Sheng et al. 1994). On the basis of such studies, it has been proposed that most Kv1-containing channels in cortex are heteromultimeric (Coleman et al. 1999; Shamotienko et al. 1997; Wang et al. 1999). This makes it difficult to determine whether specific Kv1 subunits have unique functional roles. Creation of knockout animals has addressed this, although compensation by other Kv1 subunits complicates the results (Brew et al. 2007; Smart et al. 1998).

DTX, a peptide from the venom of mamba snakes of the genus *Dendroaspi*s, is frequently used to isolate Kv1 currents due to Kv1.1, Kv1.2, or Kv1.6 α-subunits. We explicitly tested the assumption that DTX blocks all of the putative Kv1 current in layer 5 PNs. Our findings suggest that 100 nM DTX is a saturating dose and that, on average, the Kv1.3-selective blocker MTX does not block additional current after 100 nM DTX in layer 5 PNs. The lack of significant differences in the size of currents sensitive to DTX, MTX, or the combined toxins in our study suggests that DTX blocks approximately all of the Kv1 channels in layer 5 PNs and that either the majority of channels also contain Kv1.3 or MTX is not selective for Kv1.3 (cf., Bartok et al. 2014).

Consistent with the observed MTX-sensitive currents in layer 5 PNs, binding sites for the Kv1.3 blocker kaliotoxin were found in highest density in neocortex (Mourre et al. 1999). In contrast, in a nucleated patch study of large layer 5 PNs, no effect was reported for 200 nM Kv1.2- or Kv1.3-selective blockers (Korngreen and Sakmann 2000). Our data are consistent with those of Miller et al. (2008), in that they reported DTX and MTX-sensitive currents in *thy1-H*-positive PT-type PNs from mouse motor cortex. They found greater

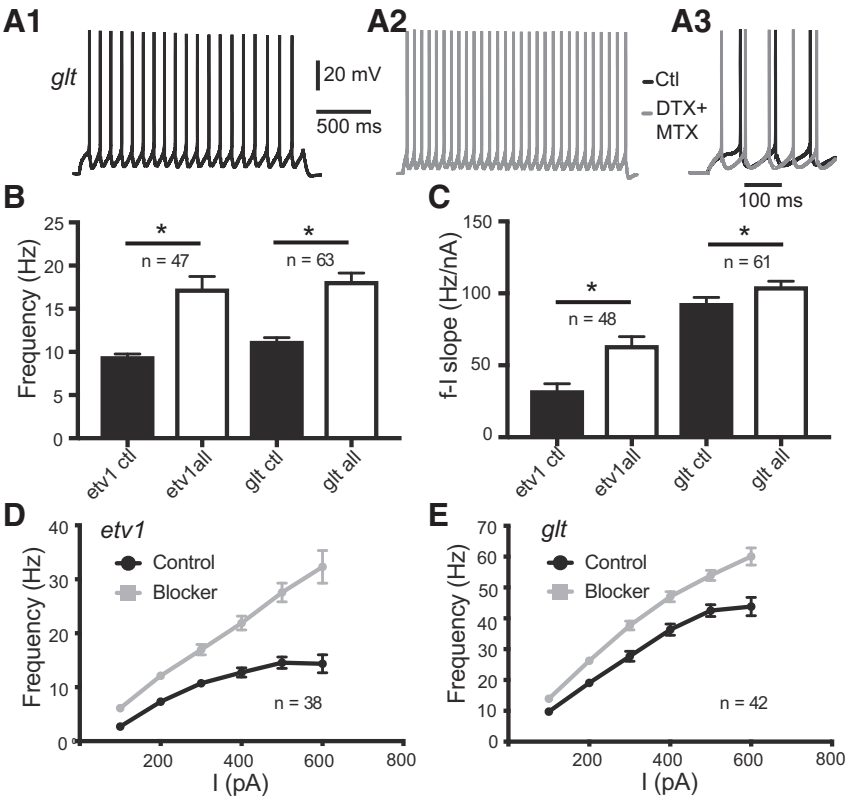

Fig. 10. Effects of Kv1 channels on gain of repetitive firing. *A1*: traces from a *glt* neuron in response to 2-s current step designed to elicit firing at ~10 Hz (100 pA and 9.5 Hz in this example) in control solution (Ctl). Scale bars apply to *A1* and *A2* (mV scale also applies to *A3*). *A2*: traces for same cell and same stimulus as in *A1*, except in the presence of 100 nM α-dendrotoxin (DTX) + 20 nM margatoxin (MTX). *A3*: initial portions of traces in *A1* and *A2* at an expanded time base to show advanced firing in DTX+MTX. *B*: summary data (means ± SE) for *etv1* and *glt* cells in response to Kv1 blockers (all = 100 nM DTX, 20 nM MTX, and DTX+MTX). $*P < 0.05$, significant difference. *C*: summary data (means ± SE) for *etv1* and *glt* cells for initial slope from linear fit to frequency-current (*f-I*) data in response to Kv1 blockers (all). $*P < 0.05$, significant difference. *D*: average *f-I* plot for 38 *etv1* cells in control solution (black) and Kv1 blockers (DTX, MTX, and DTX+MTX; gray). The *f-I* slope was significantly steeper in the Kv1 toxins ($P < 0.001$). *E*: average *f-I* plot for 42 *glt* cells in control solution (black) and Kv1 blockers (DTX, MTX, and DTX+MTX; gray). The *f-I* slope was significantly steeper in the Kv1 toxins ($P < 0.001$).

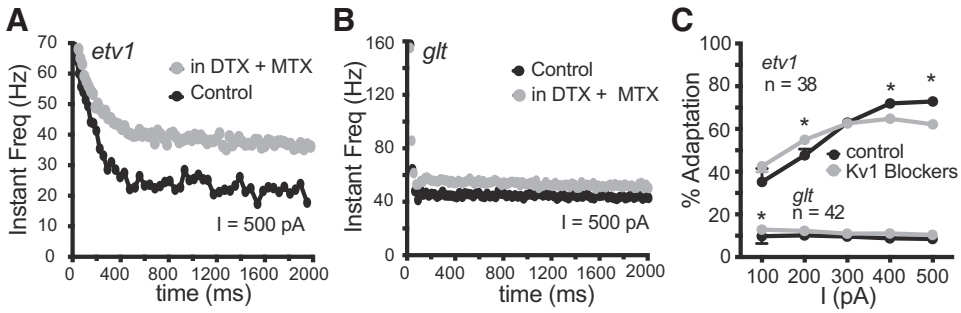

Fig. 11. Effects of Kv1 blockers on spike frequency adaptation (SFA). %SFA was defined as the ratio [(last ISI − 3rd ISI)/last ISI] × 100%, where ISI is interspike interval (see text). *A*: plot of instantaneous frequency (1/ISI) vs. time (*f-t* plot) for an *etv1* PN pyramidal neuron (PN) in control solution (black) and after 100 nM α-dendrotoxin (DTX) + 20 nM margatoxin (MTX; gray). Note smooth, slow reduction in firing rate with time in both conditions. In Kv1 blockers, firing rate was increased and SFA reduced. In this cell, %adaptation was 74% in control and 53.1% in Kv1 blockers. *B*: similar *f-t* plot for a *glt* PN. There was an initial fast SFA (ISIs 1 and 2) and very little slow SFA in control (11%). In Kv1 blockers, firing rate was increased and SFA slightly increased (to 19.1%). *C*: plot of %adaptation vs. injected current (*I*) for *etv1* and *glt* PNs in control (black) and Kv1 blockers (gray). In *etv1* PNs, %adaptation was reduced by Kv1 blockers at high currents, which are associated with faster firing. In *glt* PNs, there was a small but statistically significant increase in %adaptation with DTX+MTX at the lowest current (and firing rate).

immunocytochemical expression of Kv1 α-subunits in motor cortex vs. somatosensory cortex and observed a slowly inactivating DTX-sensitive current in whole cell voltage-clamp recordings from PNs from motor cortex but not PNs from somatosensory cortex. This latter finding differs from our observation of DTX-, MTX-, and DTX+MTX-sensitive currents in PNs from layer 5 of somatosensory cortex, perhaps reflecting a cell-type difference (all of their data were from *thy1-H*-positive cells), mouse-strain difference (theirs were C57Bl6, ours are Swiss-Webster background), or recording-condition differences (e.g., type of internal solution or whole cell vs. macropatch recording). In motor cortex, Miller et al. (2008) found that MTX blocked current with a small, rapidly inactivating component (τ ~25 ms) and a large persistent component. In contrast, the Kv1.2-selective tityustoxin blocked a current that inactivated slowly (τ ~800 ms). They suggested that at least some Kv1.2 and Kv1.3 subunits were in different channels.

Properties of Kv1 currents. We found that the putative Kv1 current was of similar amplitude in *etv1* and *glt* PNs. Overall, the Kv1-mediated current in *etv1* and *glt* PNs activated rapidly and subthreshold to AP voltage threshold, similar to previous findings in unidentified large layer 5 PNs and other cell types (Bekkers and Delaney 2001; Dodson et al. 2002; Miller et al. 2008; Shen et al. 2004) and more negative than for rat layer 2/3 PNs (Guan et al. 2006) or amygdaloid PNs (Faber and Sah 2004). The total Kv1 current consistently included both a transient and persistent component in both cell types and with all toxins. Steady-state activation voltage and kinetics were similar in *etv1* and *glt* cells, and the current sensitive to Kv1 blockers was relatively insensitive to holding potential relative to the toxin-insensitive current.

In expression systems, homomeric channels from all Kv1 α-subunits except Kv1.4 generate slowly inactivating "delayed rectifier" currents. Homomeric Kv1.4 channels are rapidly inactivating "A"-type currents, and homomeric Kv1.3 channels inactivate more completely than Kv1.1 or Kv1.2 channels (Coetzee et al. 1999; Grissmer et al. 1994; Hopkins 1998; Hopkins et al. 1994; Po et al. 1993; Ruppersberg et al. 1990). The inactivation properties of Kv1 channels can be altered by the presence of β-subunits (Monaghan et al. 2001; Morales et al. 1996; Rettig et al. 1994; Rhodes et al. 1997). Homomeric Kv1.2 channels activate more slowly and at more depolarized voltages than the others (Grissmer et al. 1994), and in native membranes, cell types with the most depolarized activation range (e.g., amygdaloid PNs) may primarily express Kv1.2 subunits (Faber and Sah 2004).

In rat layer 2/3 PNs, Kv1.1-specific toxins revealed persistent, slowly inactivating currents, Kv1.2 (tityustoxin sensitive) current exhibited a transient component in addition to the persistent component, and current sensitive to MTX inactivated at intermediate rates (Guan et al. 2006). In contrast, in mouse layer 5 PNs, we found that the biophysical properties of Kv1 currents were similar *1*) for currents sensitive to DTX, MTX, or the combined toxins and *2*) between *etv1* and *glt* PNs. An exception was that in *etv1* PNs, DTX-sensitive currents had a faster inactivation τ at +10 mV but less overall %inactivation (over 500 ms) compared with MTX-sensitive current. In *glt* PNs, the only significant difference was for activation τ, with DTX-sensitive current activating more slowly.

Differences in functional roles in etv1 and glt PNs. The amplitude and properties of Kv1-mediated currents were similar between cell types and for all Kv1 blockers. For most parameters measured, we did not find differences between effects of DTX, MTX, or the combined toxins, so we focused on the combined data for Kv1 blockers (DTX, MTX, or DTX+MTX) for functional studies. On the basis of their biophysical properties, Kv1 current should contribute to AP voltage threshold, rheobase, and regulation of firing rate in PNs. Because Kv1 channels activate in the subthreshold voltage range in PNs (Bekkers and Delaney 2001; Dodson et al. 2002; Shen et al. 2004), they are likely to play an important role in regulating cell excitability. Kv1.1 or Kv1.2 knockout mice are subject to seizures (Brew et al. 2007; Lopantsev et al. 2003; Rho et al. 1999; Smart et al. 1998), although only modest physiological changes were reported in PNs in those studies (Smart et al. 1998; van Brederode et al. 2001). Human mutations of Kv1 genes also result in seizure disorders as well as episodic ataxia (Browne et al. 1994; D'Adamo et al. 2013; Shah and Aizenman 2014; Tomlinson et al. 2010; Zuberi et al. 1999). Kv1 channels facilitate selectivity for time-varying stimuli in preference to DC inputs and regulate temporal precision and timing of APs in auditory neurons (Brew and Forsythe 1995; Dodson et al. 2002; Gittelman and Tempel

2006; Kopp-Scheinpflug et al. 2003; Kuznetsova et al. 2008; Mathews et al. 2010; Rothman and Manis 2003a, 2003b, 2003c) and neocortical PNs (Cudmore et al. 2010; Higgs and Spain 2011).

Action potential. Consistent with rat layer 2/3 PNs (Guan et al. 2007b), block of Kv1 channels resulted in a small but significant negative shift in the somatic AP voltage threshold in both *etv1* and *glt* PNs. Kv1 channels are known to regulate dynamic changes of AP voltage threshold in rat layer 2/3 PNs in response to a variety of different stimuli, including current steps and ramps of various durations, noisy current injection, or evoked synaptic inputs (Higgs and Spain 2011). DTX-sensitive Kv1 channels have previously been implicated in voltage threshold determination in rat layer 5 PNs (Bekkers and Delaney 2001) and CA1 PNs (Giglio and Storm 2014).

We found differential effects of Kv1 block on somatic AP repolarization and d*V*/d*t* between *etv1* and *glt* PNs. Consistent with our previous study, Kv1 block broadened APs and reduced d*V*/d*t* for repolarization in *etv1* but not *glt* PNs (Pathak et al. 2016). In a different PN type, Wu and Barish (1992) found that DTX caused AP broadening (CA1 PNs). In contrast, in rat layer 2/3 PNs, DTX did not affect AP width (Guan et al. 2007b). The DTX-sensitive current also had little effect on AP repolarization in CA3 pyramidal neurons (Mitterdorfer and Bean 2002) or nodose ganglia neurons (Glazebrook et al. 2002). Somatic APs were also reported to be unaffected by DTX in rat and ferret layer 5 PNs (Bekkers and Delaney 2001; Kole et al. 2007; Shu et al. 2007). In contrast, Kv1 channels play a major role regulating the AP in the axonal initial segment and axon (where there is greater expression of Kv1 currents: Kole et al. 2007; Shu et al. 2007). In dissociated CA3 neurons, the putative Kv1-mediated "D current" was activated before the peak of the AP, but not fully activated by an AP waveform (Mitterdorfer and Bean 2002; see also Guan et al. 2006).

Rheobase, latency, and repetitive firing. Kv1 block lowered rheobase and shortened the latency to the first AP in both *etv1* and *glt* PNs, similar to earlier findings in mouse layer 2/3 PNs (Guan et al. 2007b), rat layer 5 PNs (Miller et al. 2008), hippocampal PNs (Wu and Barish 1992), and striatal medium spiny cells (Nisenbaum et al. 1994; Shen et al. 2004). In rat layer 2/3 PNs (Guan et al. 2006) we found that voltage-dependent deactivation was slow at voltages corresponding to in vivo membrane potentials in the "up-state" (Cowan and Wilson 1994; Stern et al. 1997) and potentials traversed by ISIs during repetitive firing (Contreras 2004; Destexhe et al. 2003). Thus we predicted that Kv1 channels would have a major role regulating ISIs during repetitive firing.

Block of Kv1 currents resulted in lowered current required to elicit onset doublets in both *etv1* and *glt* PNs and perhaps facilitated burst firing in *glt*. We found that Kv1 block had differential effects on the gain of repetitive firing in *etv1* vs. *glt* PNs. Kv1 blockers led to significantly increased firing rate in both *etv1* and *glt* PNs. In large rat layer 5 PNs, DTX-sensitive currents also regulated firing rate (Bekkers and Delaney 2001), and several studies have shown increased firing rates by DTX in various cell types (e.g., Brew and Forsythe 1995; Chi and Nicol 2007; Faber and Sah 2004; Golding et al. 1999; Locke and Nerbonne 1997; Mitterdorfer and Bean 2002; Rothman and Manis 2003c). We found that Kv1 block also increased the initial *f-I* slope (gain) in both *etv1* and *glt* PNs; however, the magnitude of this gain change was much greater in *etv1* vs. *glt*. DTX also caused increased firing rate at all stimulus intensities in rat layer 2/3 PNs, with greater effects at larger stimulus intensities resulting in an increased gain of spike output vs. DC input (increased *f-I* slope; Guan et al. 2007b).

We observed acceleration of firing during our 2-s current injections in a small percentage of *glt* but not *etv1* PNs. In most cases Kv1 blockers eliminated this acceleration. Our finding differs from mouse motor cortex, where inactivation of a large DTX-sensitive Kv1 current in large, PT-type PNs resulted in accelerated firing in nearly all layer 5 PNs (Miller et al. 2008).

Unlike in rat layer 2/3 PNs (Guan et al. 2007b), we found an effect of Kv1 blockers on SFA in *etv1* and *glt* PNs. In *etv1* PNs, both Kv1 blockers decreased SFA to large stimuli that elicited high firing rates, whereas in *glt* PNs, the blockers increased SFA in response to the smallest stimuli only (low firing rate). In amygdaloid PNs, the DTX-sensitive current was also reported to regulate firing rate by enhancing SFA (Faber and Sah 2004). In mouse layer 2/3 PNs, developmental expression of Kv1 channels is dependent on expression of the *Cux1* gene (Rodríguez-Tornos et al. 2016). Loss of *Cux1* led to decreased expression of Kv1 transcripts, which in turn led to abnormal firing in these cells. Kv1 channels were found necessary for repetitive firing and to influence adaptation in these immature PNs, but the firing measurements in that study were dominated by the first few ISIs of short current injections and did not reflect the time course (or mechanisms) of the slow SFA previously described in neocortical PNs (Abel et al. 2004; Guan et al. 2015; Schwindt et al. 1988). Miller et al. (2008) found that DTX but not MTX blocked acceleration in layer 5 PNs from motor cortex. DTX application converted motor cortical PNs to show SFA.

Context of other currents. Despite similar expression and biophysics of Kv1 current in *etv1* and *glt* PNs, we found differences between *etv1* and *glt* PNs in terms Kv1 regulation of AP repolarization, *f-I* slope (gain), and SFA. Thus the observed firing differences do not precisely map to differences in Kv1 currents. Similarly, Dodson et al. (2002) found two Kv1 currents in neurons from the medial nucleus of the trapezoid body (MNTB): one sensitive to tityustoxin (Kv1.2) and a tityustoxin-insensitive but DTX-sensitive current. Although both currents had similar kinetic properties, only the Kv1.2-containing current was critical for generating the diagnostic single-AP pattern of firing of MNTB neurons. They suggested that this was due to only those channels being located in the axonal initial segment (AIS). Kv1 channels (especially Kv1.1 and Kv1.2) are preferentially located in the AIS of PNs and other cell types (Goldberg et al. 2008; Kole et al. 2007; Shu et al. 2007), where they control attainment of AP threshold and AP repolarization as well as control discharge patterns. It is possible that differential location of channels could contribute to differences in AP repolarization, *f-I* gain, and SFA between DTX-sensitive and MTX-sensitive channels in *etv1* and *glt* PNs (with Kv1.1 and Kv1.2 channels in the AIS and Kv1.3 channels restricted to the somatodendritic compartment), although there is no direct evidence concerning this detailed localization between cell types. In particular, differential localization may explain different responses to DTX vs. MTX on SFA in *glt* PNs.

Another possible explanation for our findings is that the cell-type differences reflect action of Kv1 channels in the context of

the other K^+ channels expressed in layer 5 PNs (these alternatives are not mutually exclusive). For example, the largest Kv component in both *etv1* and *glt* PNs is due to Kv2 channels (Bishop et al. 2015), and Kv2 current is larger in *glt* than in *etv1* PNs. Because *glt* PNs only express Kv2.1 channels and *etv1* PNs express Kv2.1 and Kv2.2, the Kv2 current activates at subthreshold voltages in *etv1* but is almost exclusively suprathreshold in *glt*. Thus, in *etv1* but not *glt* PNs, Kv2 channels should regulate rheobase. Even in *etv1* PNs, the more rapid kinetics of Kv1 currents would be expected to allow them to play a larger role in regulating voltage threshold and width of a single AP than the slower Kv2 channels. In unidentified PNs from layers 2/3 and 5, we found that Kv2 conductance is permissive for high rates of firing (knockdown of Kv2.1 resulted in slower firing; Guan et al. 2013; see also Du et al. 2000; Hönigsperger et al. 2017; Johnston et al. 2008; Liu and Bean 2014). Perhaps the reduced effect of Kv1 blockers on *f-I* slope in *glt* PNs reflects the greater importance of Kv2.1 channels in regulating firing in those cells, especially at high rates of firing.

In addition to Kv1 and Kv2 channels, repetitive firing of neocortical PNs is regulated by Kv7 (Guan et al. 2011), SK, and sAHP channels (Guan et al. 2015). Kv7 (KCNQ) channels contribute to resting membrane potential, rheobase, and firing rate (but not *f-I* slope). These channels activate slowly at subthreshold potentials and are persistent (Guan et al. 2011). Kv7 channels are also reported in layer 5 PNs (Cooper et al. 2001), and our preliminary results suggest greater expression in *etv1* than in *glt* PNs (Guan and Foehring 2015). Apamin-sensitive SK current is larger in *glt* vs. *etv1* PNs (Guan et al. 2015). Ca^{2+}-dependent K^+ channels do not contribute to AP threshold or repolarization in neocortical PNs (Abel et al. 2004; Pathak et al. 2016; Pineda et al. 1998; Schwindt et al. 1988), but SK channels do regulate firing rate without affecting *f-I* slope or SFA (Guan et al. 2015). In contrast, the sAHP current is much larger in *etv1* PNs, where it regulates ISI, firing rate, *f-I* slope, and SFA (Guan et al. 2015). The effects that we observed for Kv1 block on SFA at high firing rates in *etv1* PNs may reflect an indirect interaction between Kv1 and sAHP channels, perhaps through regulating Ca^{2+} entry.

In summary, we found evidence for differential effects of Kv1 channels on AP repolarization, gain of firing, and SFA between *etv1* and *glt* PNs, despite only minor differences in the expression and properties of Kv1 currents in these cells. It is possible that the functional differences may reflect differences in channel localization in different cell compartments or the action of Kv1 channels in the context of differences in the other K^+ channels expressed in *etv1* vs. *glt* PNs.

ACKNOWLEDGMENTS

We thank Dr. W. E. Armstrong for insightful comments on earlier versions of this manuscript.

GRANTS

This work was supported by National Institute of Neurological Disorders and Stroke Grant R01 NS044163 (to R. C. Foehring).

DISCLOSURES

No conflicts of interest, financial or otherwise, are declared by the authors.

AUTHOR CONTRIBUTIONS

D.G. and R.C.F. conceived and designed research; D.G. and D.P. performed experiments; D.G., D.P., and R.C.F. analyzed data; D.G. and R.C.F. interpreted results of experiments; D.G. and R.C.F. prepared figures; R.C.F. drafted manuscript; D.G., D.P., and R.C.F. edited and revised manuscript; R.C.F. approved final version of manuscript.

REFERENCES

Abel HJ, Lee J, Callaway JC, Foehring RC. Relationships between action potentials, afterhyperpolarizations, and calcium signaling in layer II/III neocortical pyramidal neurons. *J Neurophysiol* 91: 324–335, 2004. doi:10.1152/jn.00583.2003.

Bartok A, Toth A, Somodi S, Szanto TG, Hajdu P, Panyi G, Varga Z. Margatoxin is a non-selective inhibitor of human Kv1.3 K^+ channels. *Toxicon* 87: 6–16, 2014. doi:10.1016/j.toxicon.2014.05.002.

Bekkers JM. Properties of voltage-gated potassium currents in nucleated patches from large layer 5 cortical pyramidal neurons of the rat. *J Physiol* 525: 593–609, 2000a. doi:10.1111/j.1469-7793.2000.t01-1-00593.x.

Bekkers JM. Distribution and activation of voltage-gated potassium channels in cell-attached and outside-out patches from large layer 5 cortical pyramidal neurons of the rat. *J Physiol* 525: 611–620, 2000b. doi:10.1111/j.1469-7793.2000.t01-2-00611.x.

Bekkers JM, Delaney AJ. Modulation of excitability by alpha-dendrotoxin-sensitive potassium channels in neocortical pyramidal neurons. *J Neurosci* 21: 6553–6560, 2001. doi:10.1523/JNEUROSCI.21-17-06553.2001.

Bishop HI, Guan D, Bocksteins E, Parajuli LK, Murray KD, Cobb MM, Misonou H, Zito K, Foehring RC, Trimmer JS. Distinct, layer-specific expression patterns and independent regulation of Kv2 channel subtypes in cortical pyramidal neurons. *J Neurosci* 35: 14922–14942, 2015. doi:10.1523/JNEUROSCI.1897-15.2015.

Bossu JL, Capogna M, Debanne D, McKinney RA, Gahwhiler BH. Somatic voltage-gated potassium currents of rat hippocampal pyramidal cells in organotypic slice cultures. *J Physiol* 495: 367–381, 1996.

Brew HM, Forsythe ID. Two voltage-dependent K^+ conductances with complementary functions in postsynaptic integration at a central auditory synapse. *J Neurosci* 15: 8011–8022, 1995. doi:10.1523/JNEUROSCI.15-12-08011.1995.

Brew HM, Gittelman JX, Silverstein RS, Hanks TD, Demas VP, Robinson LC, Robbins CA, McKee-Johnson J, Chiu SY, Messing A, Tempel BL. Seizures and reduced life span in mice lacking the potassium channel subunit Kv1.2, but hypoexcitability and enlarged Kv1 currents in auditory neurons. *J Neurophysiol* 98: 1501–1525, 2007. doi:10.1152/jn.00640.2006.

Brown SP, Hestrin S. Cell-type identity: a key to unlocking the function of neocortical circuits. *Curr Opin Neurobiol* 19: 415–421, 2009. doi:10.1016/j.conb.2009.07.011.

Browne DL, Gancher ST, Nutt JG, Brunt ER, Smith EA, Kramer P, Litt M. Episodic ataxia/myokymia syndrome is associated with point mutations in the human potassium channel gene, KCNA1. *Nat Genet* 8: 136–140, 1994. doi:10.1038/ng1094-136.

Chagnac-Amitai Y, Luhmann HJ, Prince DA. Burst generating and regular spiking layer 5 pyramidal neurons of rat neocortex have different morphological features. *J Comp Neurol* 296: 598–613, 1990. doi:10.1002/cne.902960407.

Chen X, Johnston D. Properties of single voltage-dependent K^+ channels in dendrites of CA1 pyramidal neurones of rat hippocampus. *J Physiol* 559: 187–203, 2004. doi:10.1113/jphysiol.2004.068114.

Chi XX, Nicol GD. Manipulation of the potassium channel Kv1.1 and its effect on neuronal excitability in rat sensory neurons. *J Neurophysiol* 98: 2683–2692, 2007. doi:10.1152/jn.00437.2007.

Christophe E, Doerflinger N, Lavery DJ, Molnár Z, Charpak S, Audinat E. Two populations of layer V pyramidal cells of the mouse neocortex: development and sensitivity to anesthetics. *J Neurophysiol* 94: 3357–3367, 2005. doi:10.1152/jn.00076.2005.

Coetzee WA, Amarillo Y, Chiu J, Chow A, Lau D, McCormack T, Moreno H, Nadal MS, Ozaita A, Pountney D, Saganich M, Vega-Saenz de Miera E, Rudy B. Molecular diversity of K^+ channels. *Ann N Y Acad Sci* 868: 233–255, 1999. doi:10.1111/j.1749-6632.1999.tb11293.x.

Coleman SK, Newcombe J, Pryke J, Dolly JO. Subunit composition of Kv1 channels in human CNS. *J Neurochem* 73: 849–858, 1999. doi:10.1046/j.1471-4159.1999.0730849.x.

Connors BW, Gutnick MJ, Prince DA. Electrophysiological properties of neocortical neurons *in vitro*. *J Neurophysiol* 48: 1302–1320, 1982. doi:10.1152/jn.1982.48.6.1302.

Contreras D. Electrophysiological classes of neocortical neurons. *Neural Netw* 17: 633–646, 2004. doi:10.1016/j.neunet.2004.04.003.

Cooper EC, Harrington E, Jan YN, Jan LY. M channel KCNQ2 subunits are localized to key sites for control of neuronal network oscillations and synchronization in mouse brain. *J Neurosci* 21: 9529–9540, 2001. doi:10.1523/JNEUROSCI.21-24-09529.2001.

Cowan RL, Wilson CJ. Spontaneous firing patterns and axonal projections of single corticostriatal neurons in the rat medial agranular cortex. *J Neurophysiol* 71: 17–32, 1994. doi:10.1152/jn.1994.71.1.17.

Cudmore RH, Fronzaroli-Molinieres L, Giraud P, Debanne D. Spike-time precision and network synchrony are controlled by the homeostatic regulation of the D-type potassium current. *J Neurosci* 30: 12885–12895, 2010. doi:10.1523/JNEUROSCI.0740-10.2010.

D'Adamo MC, Catacuzzeno L, Di Giovanni G, Franciolini F, Pessia M. K^+ channelepsy: progress in the neurobiology of potassium channels and epilepsy. *Front Cell Neurosci* 7: 134, 2013. doi:10.3389/fncel.2013.00134.

Dembrow NC, Chitwood RA, Johnston D. Projection-specific neuromodulation of medial prefrontal cortex neurons. *J Neurosci* 30: 16922–16937, 2010. doi:10.1523/JNEUROSCI.3644-10.2010.

Destexhe A, Rudolph M, Paré D. The high-conductance state of neocortical neurons in vivo. *Nat Rev Neurosci* 4: 739–751, 2003. [Erratum in *Nat Rev Neurosci* 4: 1019, 2003]. doi:10.1038/nrn1198.

Dodson PD, Barker MC, Forsythe ID. Two heteromeric Kv1 potassium channels differentially regulate action potential firing. *J Neurosci* 22: 6953–6961, 2002. doi:10.1523/JNEUROSCI.22-16-06953.2002.

Dodt HU, Zieglgänsberger W. Visualizing unstained neurons in living brain slices by infrared DIC-videomicroscopy. *Brain Res* 537: 333–336, 1990. doi:10.1016/0006-8993(90)90380-T.

Dong Y, White FJ. Dopamine D1-class receptors selectively modulate a slowly inactivating potassium current in rat medial prefrontal cortex pyramidal neurons. *J Neurosci* 23: 2686–2695, 2003. doi:10.1523/JNEUROSCI.23-07-02686.2003.

Doyle JP, Dougherty JD, Heiman M, Schmidt EF, Stevens TR, Ma G, Bupp S, Shrestha P, Shah RD, Doughty ML, Gong S, Greengard P, Heintz N. Application of a translational profiling approach for the comparative analysis of CNS cell types. *Cell* 135: 749–762, 2008. doi:10.1016/j.cell.2008.10.029.

Du J, Haak LL, Phillips-Tansey E, Russell JT, McBain CJ. Frequency-dependent regulation of rat hippocampal somato-dendritic excitability by the K^+ channel subunit Kv2.1. *J Physiol* 522: 19–31, 2000. doi:10.1111/j.1469-7793.2000.t01-2-00019.xm.

Faber ES, Sah P. Opioids inhibit lateral amygdala pyramidal neurons by enhancing a dendritic potassium current. *J Neurosci* 24: 3031–3039, 2004. doi:10.1523/JNEUROSCI.4496-03.2004.

Foehring RC, Surmeier DJ. Voltage-gated potassium currents in acutely dissociated rat cortical neurons. *J Neurophysiol* 70: 51–63, 1993. doi:10.1152/jn.1993.70.1.51.

Giglio AM, Storm JF. Postnatal development of temporal integration, spike timing and spike threshold regulation by a dendrotoxin-sensitive K^+ current in rat CA1 hippocampal cells. *Eur J Neurosci* 39: 12–23, 2014. doi:10.1111/ejn.12385.

Gittelman JX, Tempel BL. Kv1.1-containing channels are critical for temporal precision during spike initiation. *J Neurophysiol* 96: 1203–1214, 2006. doi:10.1152/jn.00092.2005.

Glazebrook PA, Ramirez AN, Schild JH, Shieh CC, Doan T, Wible BA, Kunze DL. Potassium channels Kv1.1, Kv1.2 and Kv1.6 influence excitability of rat visceral sensory neurons. *J Physiol* 541: 467–482, 2002. doi:10.1113/jphysiol.2001.018333.

Goldberg EM, Clark BD, Zagha E, Nahmani M, Erisir A, Rudy B. K^+ channels at the axon initial segment dampen near-threshold excitability of neocortical fast-spiking GABAergic interneurons. *Neuron* 58: 387–400, 2008. doi:10.1016/j.neuron.2008.03.003.

Golding NL, Jung HY, Mickus T, Spruston N. Dendritic calcium spike initiation and repolarization are controlled by distinct potassium channel subtypes in CA1 pyramidal neurons. *J Neurosci* 19: 8789–8798, 1999. doi:10.1523/JNEUROSCI.19-20-08789.1999.

Gong S, Doughty M, Harbaugh CR, Cummins A, Hatten ME, Heintz N, Gerfen CR. Targeting Cre recombinase to specific neuron populations with bacterial artificial chromosome constructs. *J Neurosci* 27: 9817–9823, 2007. doi:10.1523/JNEUROSCI.2707-07.2007.

Gong S, Yang XW, Li C, Heintz N. Highly efficient modification of bacterial artificial chromosomes (BACs) using novel shuttle vectors containing the R6Kgamma origin of replication. *Genome Res* 12: 1992–1998, 2002. doi:10.1101/gr.476202.

Gong S, Zheng C, Doughty ML, Losos K, Didkovsky N, Schambra UB, Nowak NJ, Joyner A, Leblanc G, Hatten ME, Heintz N. A gene expression atlas of the central nervous system based on bacterial artificial chromosomes. *Nature* 425: 917–925, 2003. doi:10.1038/nature02033.

Grissmer S, Nguyen AN, Aiyar J, Hanson DC, Mather RJ, Gutman GA, Karmilowicz MJ, Auperin DD, Chandy KG. Pharmacological characterization of five cloned voltage-gated K^+ channels, types Kv1.1, 1.2, 1.3, 1.5, and 3.1, stably expressed in mammalian cell lines. *Mol Pharmacol* 45: 1227–1234, 1994.

Groh A, Meyer HS, Schmidt EF, Heintz N, Sakmann B, Krieger P. Cell-type specific properties of pyramidal neurons in neocortex underlying a layout that is modifiable depending on the cortical area. *Cereb Cortex* 20: 826–836, 2010. doi:10.1093/cercor/bhp152.

Guan D, Armstrong WE, Foehring RC. Kv2 channels regulate firing rate in pyramidal neurons from rat sensorimotor cortex. *J Physiol* 591: 4807–4825, 2013. doi:10.1113/jphysiol.2013.257253.

Guan D, Armstrong WE, Foehring RC. Electrophysiological properties of genetically identified subtypes of layer 5 neocortical pyramidal neurons: Ca^{2+} dependence and differential modulation by norepinephrine. *J Neurophysiol* 113: 2014–2032, 2015. doi:10.1152/jn.00524.2014.

Guan D, Foehring RC. Differential expression of voltage-gated potassium conductances in genetically-defined layer 5 neocortical pyramidal neurons. Program No. 121.29. *2015 Neuroscience Meeting Planner*. Chicago, IL: Society for Neuroscience, 2015.

Guan D, Higgs MH, Horton LR, Spain WJ, Foehring RC. Contributions of Kv7-mediated potassium current to sub- and suprathreshold responses of rat layer II/III neocortical pyramidal neurons. *J Neurophysiol* 106: 1722–1733, 2011a. doi:10.1152/jn.00211.2011.

Guan D, Horton LR, Armstrong WE, Foehring RC. Postnatal development of A-type and Kv1- and Kv2-mediated potassium channel currents in neocortical pyramidal neurons. *J Neurophysiol* 105: 2976–2988, 2011b. doi:10.1152/jn.00758.2010.

Guan D, Lee JC, Higgs M, Spain WJ, Foehring RC. Functional roles of Kv1 channels in neocortical pyramidal neurons. *J Neurophysiol* 97: 1931–1940, 2007b. 10.1152/jn.00933.2006.

Guan D, Lee JC, Tkatch T, Surmeier DJ, Armstrong WE, Foehring RC. Expression and biophysical properties of Kv1 channels in supragranular neocortical pyramidal neurons. *J Physiol* 571: 371–389, 2006. [Erratum in *J Physiol* 572: 307, 2006.] doi:10.1113/jphysiol.2005.097006.

Guan D, Tkatch T, Surmeier DJ, Armstrong WE, Foehring RC. Kv2 subunits underlie slowly inactivating potassium current in rat neocortical pyramidal neurons. *J Physiol* 581: 941–960, 2007a. doi:10.1113/jphysiol.2007.128454.

Halliwell JV, Othman IB, Pelchen-Matthews A, Dolly JO. Central action of dendrotoxin: selective reduction of a transient K conductance in hippocampus and binding to localized acceptors. *Proc Natl Acad Sci USA* 83: 493–497, 1986. doi:10.1073/pnas.83.2.493.

Harvey AL, Robertson B. Dendrotoxins: structure-activity relationships and effects on potassium ion channels. *Curr Med Chem* 11: 3065–3072, 2004. doi:10.2174/0929867043363820.

Hattox AM, Nelson SB. Layer V neurons in mouse cortex projecting to different targets have distinct physiological properties. *J Neurophysiol* 98: 3330–3340, 2007. doi:10.1152/jn.00397.2007.

Heinemann SH, Rettig J, Graack HR, Pongs O. Functional characterization of Kv channel beta-subunits from rat brain. *J Physiol* 493: 625–633, 1996. doi:10.1113/jphysiol.1996.sp021409.

Higgs MH, Spain WJ. Kv1 channels control spike threshold dynamics and spike timing in cortical pyramidal neurones. *J Physiol* 589: 5125–5142, 2011. doi:10.1113/jphysiol.2011.216721.

Hönigsperger C, Nigro MJ, Storm JF. Physiological roles of Kv2 channels in entorhinal cortex layer II stellate cells revealed by Guangxitoxin-1E. *J Physiol* 595: 739–757, 2017. doi:10.1113/JP273024.

Hopkins WF. Toxin and subunit specificity of blocking affinity of three peptide toxins for heteromultimeric, voltage-gated potassium channels expressed in *Xenopus* oocytes. *J Pharmacol Exp Ther* 285: 1051–1060, 1998.

Hopkins WF, Allen ML, Houamed KM, Tempel BL. Properties of voltage-gated K^+ currents expressed in *Xenopus* oocytes by mKv1.1, mKv1.2 and their heteromultimers as revealed by mutagenesis of the dendrotoxin-binding site in mKv1.1. *Pflugers Arch* 428: 382–390, 1994. doi:10.1007/BF00724522.

Ivy GO, Killackey HP. Ontogenetic changes in the projections of neocortical neurons. *J Neurosci* 2: 735–743, 1982. doi:10.1523/JNEUROSCI.02-06-00735.1982.

Johnston J, Griffin SJ, Baker C, Skrzypiec A, Chernova T, Forsythe ID. Initial segment Kv2.2 channels mediate a slow delayed rectifier and maintain high frequency action potential firing in medial nucleus of the trapezoid

body neurons. *J Physiol* 586: 3493–3509, 2008. doi:10.1113/jphysiol.2008.153734.

Kasper EM, Larkman AU, Lübke J, Blakemore C. Pyramidal neurons in layer 5 of the rat visual cortex. I. Correlation among cell morphology, intrinsic electrophysiological properties, and axon targets. *J Comp Neurol* 339: 459–474, 1994. doi:10.1002/cne.903390402.

Kim EJ, Juavinett AL, Kyubwa EM, Jacobs MW, Callaway EM. Three types of cortical layer 5 neurons that differ in brain-wide connectivity and function. *Neuron* 88: 1253–1267, 2015. doi:10.1016/j.neuron.2015.11.002.

Kole MH, Letzkus JJ, Stuart GJ. Axon initial segment Kv1 channels control axonal action potential waveform and synaptic efficacy. *Neuron* 55: 633–647, 2007. doi:10.1016/j.neuron.2007.07.031.

Kopp-Scheinpflug C, Fuchs K, Lippe WR, Tempel BL, Rübsamen R. Decreased temporal precision of auditory signaling in Kcna1-null mice: an electrophysiological study in vivo. *J Neurosci* 23: 9199–9207, 2003. doi:10.1523/JNEUROSCI.23-27-09199.2003.

Korngreen A, Sakmann B. Voltage-gated K^+ channels in layer 5 neocortical pyramidal neurones from young rats: subtypes and gradients. *J Physiol* 525: 621–639, 2000. doi:10.1111/j.1469-7793.2000.00621.x.

Kuznetsova MS, Higgs MH, Spain WJ. Adaptation of firing rate and spike-timing precision in the avian cochlear nucleus. *J Neurosci* 28: 11906–11915, 2008. doi:10.1523/JNEUROSCI.3827-08.2008.

Larkman A, Mason A. Correlations between morphology and electrophysiology of pyramidal neurons in slices of rat visual cortex. I. Establishment of cell classes. *J Neurosci* 10: 1407–1414, 1990. doi:10.1523/JNEUROSCI.10-05-01407.1990.

Le Bé JV, Silberberg G, Wang Y, Markram H. Morphological, electrophysiological, and synaptic properties of corticocallosal pyramidal cells in the neonatal rat neocortex. *Cereb Cortex* 17: 2204–2213, 2007. doi:10.1093/cercor/bhl127.

Liu PW, Bean BP. Kv2 channel regulation of action potential repolarization and firing patterns in superior cervical ganglion neurons and hippocampal CA1 pyramidal neurons. *J Neurosci* 34: 4991–5002, 2014. doi:10.1523/JNEUROSCI.1925-13.2014.

Locke RE, Nerbonne JM. Role of voltage-gated K^+ currents in mediating the regular-spiking phenotype of callosal-projecting rat visual cortical neurons. *J Neurophysiol* 78: 2321–2335, 1997. doi:10.1152/jn.1997.78.5.2321.

Lopantsev V, Tempel BL, Schwartzkroin PA. Hyperexcitability of CA3 pyramidal cells in mice lacking the potassium channel subunit Kv1.1. *Epilepsia* 44: 1506–1512, 2003. doi:10.1111/j.0013-9580.2003.44602.x.

Mason A, Larkman A. Correlations between morphology and electrophysiology of pyramidal neurons in slices of rat visual cortex. II. Electrophysiology. *J Neurosci* 10: 1415–1428, 1990. doi:10.1523/JNEUROSCI.10-05-01415.1990.

Mathews PJ, Jercog PE, Rinzel J, Scott LL, Golding NL. Control of submillisecond synaptic timing in binaural coincidence detectors by K_v1 channels. *Nat Neurosci* 13: 601–609, 2010. doi:10.1038/nn.2530.

Metz AE, Spruston N, Martina M. Dendritic D-type potassium currents inhibit the spike afterdepolarization in rat hippocampal CA1 pyramidal neurons. *J Physiol* 581: 175–187, 2007. doi:10.1113/jphysiol.2006.127068.

Miller MN, Okaty BW, Nelson SB. Region-specific spike-frequency acceleration in layer 5 pyramidal neurons mediated by Kv1 subunits. *J Neurosci* 28: 13716–13726, 2008. doi:10.1523/JNEUROSCI.2940-08.2008.

Mitterdorfer J, Bean BP. Potassium currents during the action potential of hippocampal CA3 neurons. *J Neurosci* 22: 10106–10115, 2002. doi:10.1523/JNEUROSCI.22-23-10106.2002.

Monaghan MM, Trimmer JS, Rhodes KJ. Experimental localization of Kv1 family voltage-gated K^+ channel alpha and beta subunits in rat hippocampal formation. *J Neurosci* 21: 5973–5983, 2001. doi:10.1523/JNEUROSCI.21-16-05973.2001.

Morales MJ, Wee JO, Wang S, Strauss HC, Rasmusson RL. The N-terminal domain of a K^+ channel beta subunit increases the rate of C-type inactivation from the cytoplasmic side of the channel. *Proc Natl Acad Sci USA* 93: 15119–15123, 1996. doi:10.1073/pnas.93.26.15119.

Mourre C, Chernova MN, Martin-Eauclaire MF, Bessone R, Jacquet G, Gola M, Alper SL, Crest M. Distribution in rat brain of binding sites of kaliotoxin, a blocker of Kv1.1 and Kv1.3 alpha-subunits. *J Pharmacol Exp Ther* 291: 943–952, 1999.

Murakoshi H, Trimmer JS. Identification of the Kv2.1 K^+ channel as a major component of the delayed rectifier K^+ current in rat hippocampal neurons. *J Neurosci* 19: 1728–1735, 1999. doi:10.1523/JNEUROSCI.19-05-01728.1999.

Nisenbaum ES, Xu ZC, Wilson CJ. Contribution of a slowly inactivating potassium current to the transition to firing of neostriatal spiny projection neurons. *J Neurophysiol* 71: 1174–1189, 1994. doi:10.1152/jn.1994.71.3.1174.

Pathak D, Guan D, Foehring RC. Roles of specific Kv channel types in repolarization of the action potential in genetically identified subclasses of pyramidal neurons in mouse neocortex. *J Neurophysiol* 115: 2317–2329, 2016. doi:10.1152/jn.01028.2015.

Pineda JC, Waters RS, Foehring RC. Specificity in the interaction of HVA Ca^{2+} channel types with Ca^{2+}-dependent AHPs and firing behavior in neocortical pyramidal neurons. *J Neurophysiol* 79: 2522–2534, 1998. doi:10.1152/jn.1998.79.5.2522.

Po S, Roberds S, Snyders DJ, Tamkun MM, Bennett PB. Heteromultimeric assembly of human potassium channels. Molecular basis of a transient outward current? *Circ Res* 72: 1326–1336, 1993. doi:10.1161/01.RES.72.6.1326.

Reiner A, Hart NM, Lei W, Deng Y. Corticostriatal projection neurons—dichotomous types and dichotomous functions. *Front Neuroanat* 4: 142, 2010. doi:10.3389/fnana.2010.00142.

Reiner A, Jiao Y, Del Mar N, Laverghetta AV, Lei WL. Differential morphology of pyramidal tract-type and intratelencephalically projecting-type corticostriatal neurons and their intrastriatal terminals in rats. *J Comp Neurol* 457: 420–440, 2003. doi:10.1002/cne.10541.

Rettig J, Heinemann SH, Wunder F, Lorra C, Parcej DN, Dolly JO, Pongs O. Inactivation properties of voltage-gated K^+ channels altered by presence of beta-subunit. *Nature* 369: 289–294, 1994. doi:10.1038/369289a0.

Rho JM, Szot P, Tempel BL, Schwartzkroin PA. Developmental seizure susceptibility of Kv1.1 potassium channel knockout mice. *Dev Neurosci* 21: 320–327, 1999. doi:10.1159/000017381.

Rhodes KJ, Strassle BW, Monaghan MM, Bekele-Arcuri Z, Matos MF, Trimmer JS. Association and colocalization of the Kvbeta1 and Kvbeta2 beta-subunits with Kv1 alpha-subunits in mammalian brain K^+ channel complexes. *J Neurosci* 17: 8246–8258, 1997. doi:10.1523/JNEUROSCI.17-21-08246.1997.

Rodríguez-Tornos FM, Briz CG, Weiss LA, Sebastián-Serrano A, Ares S, Navarrete M, Frangeul L, Galazo M, Jabaudon D, Esteban JA, Nieto M. *Cux1* enables interhemispheric connections of layer II/III neurons by regulating Kv1-dependent firing. *Neuron* 89: 494–506, 2016. doi:10.1016/j.neuron.2015.12.020.

Rothman JS, Manis PB. Differential expression of three distinct potassium currents in the ventral cochlear nucleus. *J Neurophysiol* 89: 3070–3082, 2003a. doi:10.1152/jn.00125.2002.

Rothman JS, Manis PB. Kinetic analyses of three distinct potassium conductances in ventral cochlear nucleus neurons. *J Neurophysiol* 89: 3083–3096, 2003b. doi:10.1152/jn.00126.2002.

Rothman JS, Manis PB. The roles potassium currents play in regulating the electrical activity of ventral cochlear nucleus neurons. *J Neurophysiol* 89: 3097–3113, 2003c. doi:10.1152/jn.00127.2002.

Ruppersberg JP, Schröter KH, Sakmann B, Stocker M, Sewing S, Pongs O. Heteromultimeric channels formed by rat brain potassium-channel proteins. *Nature* 345: 535–537, 1990. doi:10.1038/345535a0.

Salkoff L, Baker K, Butler A, Covarrubias M, Pak MD, Wei A. An essential 'set' of K^+ channels conserved in flies, mice and humans. *Trends Neurosci* 15: 161–166, 1992. doi:10.1016/0166-2236(92)90165-5.

Schmidt EF, Warner-Schmidt JL, Otopalik BG, Pickett SB, Greengard P, Heintz N. Identification of the cortical neurons that mediate antidepressant responses. *Cell* 149: 1152–1163, 2012. doi:10.1016/j.cell.2012.03.038.

Schwindt PC, Spain WJ, Foehring RC, Chubb MC, Crill WE. Slow conductances in neurons from cat sensorimotor cortex in vitro and their role in slow excitability changes. *J Neurophysiol* 59: 450–467, 1988. doi:10.1152/jn.1988.59.2.450.

Scott VE, Muniz ZM, Sewing S, Lichtinghagen R, Parcej DN, Pongs O, Dolly JO. Antibodies specific for distinct Kv subunits unveil a heterooligomeric basis for subtypes of alpha-dendrotoxin-sensitive K^+ channels in bovine brain. *Biochemistry* 33: 1617–1623, 1994. doi:10.1021/bi00173a001.

Shah NH, Aizenman E. Voltage-gated potassium channels at the crossroads of neuronal function, ischemic tolerance, and neurodegeneration. *Transl Stroke Res* 5: 38–58, 2014. doi:10.1007/s12975-013-0297-7.

Shamotienko OG, Parcej DN, Dolly JO. Subunit combinations defined for K^+ channel Kv1 subtypes in synaptic membranes from bovine brain. *Biochemistry* 36: 8195–8201, 1997. doi:10.1021/bi970237g.

Sheets PL, Suter BA, Kiritani T, Chan CS, Surmeier DJ, Shepherd GM. Corticospinal-specific HCN expression in mouse motor cortex: I_h-dependent synaptic integration as a candidate microcircuit mechanism involved in motor control. *J Neurophysiol* 106: 2216–2231, 2011. doi:10.1152/jn.00232.2011.

Shen W, Hernandez-Lopez S, Tkatch T, Held JE, Surmeier DJ. Kv1.2-containing K^+ channels regulate subthreshold excitability of striatal medium spiny neurons. *J Neurophysiol* 91: 1337–1349, 2004. doi:10.1152/jn.00414.2003.

Sheng M, Tsaur ML, Jan YN, Jan LY. Contrasting subcellular localization of the Kv1.2 K^+ channel subunit in different neurons of rat brain. *J Neurosci* 14: 2408–2417, 1994. doi:10.1523/JNEUROSCI.14-04-02408.1994.

Shepherd GM. Corticostriatal connectivity and its role in disease. *Nat Rev Neurosci* 14: 278–291, 2013. doi:10.1038/nrn3469.

Shu Y, Yu Y, Yang J, McCormick DA. Selective control of cortical axonal spikes by a slowly inactivating K^+ current. *Proc Natl Acad Sci USA* 104: 11453–11458, 2007. doi:10.1073/pnas.0702041104.

Smart SL, Lopantsev V, Zhang CL, Robbins CA, Wang H, Chiu SY, Schwartzkroin PA. Messing A, Tempel BL. Deletion of the $K_V1.1$ channels causes epilepsy in mice. *Neuron* 20: 809–819, 1998. doi:10.1016/S0896-6273(00)81018-1.

Stern EA, Kincaid AE, Wilson CJ. Spontaneous subthreshold membrane potential fluctuations and action potential variability of rat corticostriatal and striatal neurons in vivo. *J Neurophysiol* 77: 1697–1715, 1997. doi:10.1152/jn.1997.77.4.1697.

Stuart GJ, Dodt HU, Sakmann B. Patch-clamp recordings from the soma and dendrites of neurons in brain slices using infrared video microscopy. *Pflugers Arch* 423: 511–518, 1993. doi:10.1007/BF00374949.

Suter BA, Migliore M, Shepherd GM. Intrinsic electrophysiology of mouse corticospinal neurons: a class-specific triad of spike-related properties. *Cereb Cortex* 23: 1965–1977, 2013. doi:10.1093/cercor/bhs184.

Tomlinson SE, Tan SV, Kullmann DM, Griggs RC, Burke D, Hanna MG, Bostock H. Nerve excitability studies characterize Kv1.1 fast potassium channel dysfunction in patients with episodic ataxia type 1. *Brain* 133: 3530–3540, 2010. doi:10.1093/brain/awq318.

Tseng GF, Prince DA. Heterogeneity of rat corticospinal neurons. *J Comp Neurol* 335: 92–108, 1993. doi:10.1002/cne.903350107.

van Brederode JF, Rho JM, Cerne R, Tempel BL, Spain WJ. Evidence of altered inhibition in layer V pyramidal neurons from neocortex of Kcna1-null mice. *Neuroscience* 103: 921–929, 2001. doi:10.1016/S0306-4522(01)00041-0.

Wang FC, Parcej DN, Dolly JO. α-Subunit compositions of Kv1.1-containing K^+ channel subtypes fractionated from rat brain using dendrotoxins. *Eur J Biochem* 263: 230–237, 1999. doi:10.1046/j.1432-1327.1999.00493.x.

Wang H, Kunkel DD, Martin TM, Schwartzkroin PA, Tempel BL. Heteromultimeric K^+ channels in terminal and juxtaparanodal regions of neurons. *Nature* 365: 75–79, 1993. doi:10.1038/365075a0.

Wang H, Kunkel DD, Schwartzkroin PA, Tempel BL. Localization of Kv1.1 and Kv1.2, two K channel proteins, to synaptic terminals, somata, and dendrites in the mouse brain. *J Neurosci* 14: 4588–4599, 1994. doi:10.1523/JNEUROSCI.14-08-04588.1994.

Wise SP, Jones EG. Cells of origin and terminal distribution of descending projections of the rat somatic sensory cortex. *J Comp Neurol* 175: 129–157, 1977. doi:10.1002/cne.901750202.

Wu RL, Barish ME. Two pharmacologically and kinetically distinct transient potassium currents in cultured embryonic mouse hippocampal neurons. *J Neurosci* 12: 2235–2246, 1992. doi:10.1523/JNEUROSCI.12-06-02235.1992.

Zhou FM, Hablitz JJ. Layer I neurons of the rat neocortex. II. Voltage-dependent outward currents. *J Neurophysiol* 76: 668–682, 1996. doi:10.1152/jn.1996.76.2.668.

Zuberi SM, Eunson LH, Spauschus A, De Silva R, Tolmie J, Wood NW, McWilliam RC, Stephenson JB, Kullmann DM, Hanna MG. A novel mutation in the human voltage-gated potassium channel gene (Kv1.1) associates with episodic ataxia type 1 and sometimes with partial epilepsy. *Brain* 122: 817–825, 1999. doi:10.1093/brain/122.5.817.